

Most Hot Jupiters Were Cool Giant Planets for More Than 1 Gyr

STEPHEN P. SCHMIDT  ^{1,*} AND KEVIN C. SCHLAUFMAN  ¹

¹ *William H. Miller III Department of Physics & Astronomy, Johns Hopkins University, 3400 N Charles Street, Baltimore, MD 21218, USA*

(Received August 19, 2025; Revised January 22, 2026)

Submitted to AAS Journals

ABSTRACT

The origin of hot Jupiters is the oldest problem in exoplanet astrophysics. Hot Jupiters formed in situ or via disk migration should be in place just a few Myr after the formation of their host stars. On the other hand, hot Jupiters formed via eccentricity excitation and tidal damping as a result of planet–planet scattering or Kozai–Lidov oscillations may take 1 Gyr or more to arrive at their observed locations. We propose that the relative ages of hot Jupiters inside, near, and outside the bias-corrected peak of the observed hot Jupiter period distribution can be used to distinguish between these possibilities. Though the lack of precise and accurate age inferences for isolated hot Jupiter host stars makes this test difficult to implement, comparisons between the Galactic velocity dispersions of the hot Jupiter subpopulations enable this investigation. To transform relative age offsets into absolute age offsets, we calibrate the monotonically increasing solar neighborhood age–velocity dispersion relation using an all-sky sample of subgiants with precise ages and a metallicity distribution matched to that of hot Jupiter hosts. We find that the inside-peak and near-peak subpopulations are older than the outside-peak subpopulation, with the inside-peak subpopulation slightly older than the near-peak subpopulation. We conclude that at least 40% but not more than 70% of the hot Jupiter population must have formed via a late-time, peak-populating process like high-eccentricity migration that typically occurs more than 1.5 Gyr after system formation.

Keywords: Exoplanet dynamics (490) — Exoplanet evolution (491) — Exoplanet formation (492) — Exoplanet migration (2205) — Exoplanets (498) — Stellar kinematics (1608)

1. INTRODUCTION

Giant planets with orbital periods $P_{\text{orb}} < 10$ d (i.e., hot Jupiters) form either in situ or at longer orbital periods. In situ formation requires massive or high dust-to-gas ratio protoplanetary disks (e.g., P. Bodenheimer et al. 2000; K. Batygin et al. 2016). In protoplanetary disks more similar to the minimum-mass solar nebula however, giant planet formation is expected take place at wider separations potentially beyond a protoplanetary disk’s water-ice line (e.g., J. B. Pollack et al. 1996; O. Hubickyj et al. 2005). These giant planets on wide-separation orbits only become hot Jupiters if they experience inward migration. This inward migration can happen promptly as a result of interactions with a newly

formed planet’s parent protoplanetary disk (e.g., W. R. Ward 1997; D. N. C. Lin et al. 1996). Alternatively, this migration can occur after the era of the protoplanetary disk as a result of planet–planet scattering (e.g., F. A. Rasio & E. B. Ford 1996; S. J. Weidenschilling & F. Marzari 1996) or Kozai–Lidov oscillations caused by a wide-separation stellar- or planetary-mass companion exciting the proto-hot Jupiter’s eccentricity (e.g., M. Holman et al. 1997; T. Mazeh et al. 1997; L. G. Kiseleva et al. 1998; Y. Wu & N. Murray 2003; M. Nagasawa et al. 2008; D. J. Muñoz et al. 2016). Scattering events can occur promptly after the dissipation of the parent protoplanetary disk or at late times (e.g., C. Beaugé & D. Nesvorný 2012; Y. Wu & Y. Lithwick 2011), while Kozai–Lidov oscillations always occur on secular timescales. Tidal evolution also occurs on secular timescales, with dissipation inside the planet circularizing its orbit and aligning its rotation with the orbit’s angular momentum. In parallel, dissipation inside

Corresponding author: Stephen P. Schmidt

Email: sschmi42@jhu.edu

* NSF Graduate Research Fellow

the star aligns its rotation with the orbit's angular momentum and causes the orbit's semimajor axis to shrink (e.g., F. A. Rasio et al. 1996; B. Jackson et al. 2008; J. Leconte et al. 2010). These mechanisms make differing predictions for the timescale of hot Jupiter formation as well as the subsequent evolution of hot Jupiter systems.

The observed distribution of orbital parameters for hot Jupiter systems have provided some insight into their formation pathways. Studies of their semimajor axis distribution (e.g., P. Plavchan & C. Bilinski 2013; B. E. Nelson et al. 2017), their eccentricity distribution (e.g., C. Petrovich 2015), or both (e.g., A. S. Bonomo et al. 2017) suggest that high-eccentricity migration can explain most or all hot Jupiters within their selected samples. Likewise, studies of the hot Jupiter host star sky-projected obliquity distribution indicate that high-eccentricity migration is a major (or even sole) contributor to the hot Jupiter population (e.g., D. C. Fabrycky & J. N. Winn 2009; T. D. Morton & J. A. Johnson 2011; S. Naoz et al. 2012; M. Rice et al. 2022a).

On the other hand, studies of the occurrence of wider-separation stellar- or planetary-mass companions to hot Jupiters indicate that many hot Jupiter systems lack perturbers capable of inducing high-eccentricity migration (H. A. Knutson et al. 2014; M. L. Bryan et al. 2016; H. Ngo et al. 2016; K. C. Schlaufman & J. N. Winn 2016). Though some individual systems show evidence for high eccentricity migration (e.g., D. Naef et al. 2001; Y. Wu & N. Murray 2003; A. F. Gupta et al. 2024), other systems have architectures impossible to reconcile with high-eccentricity migration (e.g., J. C. Becker et al. 2015; B. J. Hord et al. 2022). While these studies have provided insight into the formation of hot Jupiters, inconsistencies still exist and new approaches are needed to ultimately resolve hot Jupiter formation.

New techniques that provide access to the time evolution of hot Jupiter systems have recently been used to constrain their eventual fates. J. H. Hamer & K. C. Schlaufman (2019) used a sample of solar neighborhood hot Jupiters available at that time to show that the Galactic velocity dispersion of their host stars was much colder than matched control samples of field stars, suggesting that the hot Jupiter population is relatively young as a consequence of the tidal destruction of the oldest and smallest-separation systems. This result was independently confirmed by S. Miyazaki & K. Masuda (2023) and D.-C. Chen et al. (2023). J. H. Hamer & K. C. Schlaufman (2020) subsequently obtained similar results for Kepler-discovered hot Jupiters.

More recent population age calculations have moved beyond studying the fates of hot Jupiters towards the time evolution of planetary systems. J. H. Hamer &

K. C. Schlaufman (2022) showed that misaligned hot Jupiter systems have a warmer velocity dispersion than aligned systems. They interpreted this observation as evidence that hot Jupiters that formed via a process that increases host star obliquity arrived later than hot Jupiters formed via a process that favors low host star obliquities. This approach becomes even more powerful if the age–velocity dispersion relation can be calibrated to provide absolute population age as a function of Galactic velocity dispersion. S. P. Schmidt et al. (2024) calibrated the age–velocity dispersion relation in the Kepler field and showed that ultra-short-period planets arrived at their observed locations after billions of years of tidal migration.

A calibrated solar neighborhood age–velocity dispersion relation could be used to study the formation time evolution of hot Jupiter systems more precisely than previously possible. A hot Jupiter population formed primarily via in situ formation or disk migration would include systems as young as a few Myr. On the other hand, planet–planet scattering need not take place immediately after the dissipation of planetary systems' parent protoplanetary disks. Similarly, Kozai–Lidov oscillations occur only on secular timescales. As a result, a hot Jupiter population formed primarily via high-eccentricity migration could have relatively fewer younger systems and an older average age than a population formed primarily in situ or via disk migration. Subsequent tidal dissipation can also affect the observed mean ages of the smallest-separation hot Jupiter systems.

To clarify the relative importance of these formation mechanisms for the overall hot Jupiter population, we propose to compare the characteristic mean ages of different hot Jupiter subpopulations as illustrated in Figure 1. We first subdivide the overall hot Jupiter population into three subpopulations based on their proximity to the peak of the orbital period distribution after accounting for observation biases: (1) an inside-peak subpopulation, (2) a near-peak subpopulation, and (3) an outside-peak subpopulation. If an early time mechanism like disk migration or in situ formation is responsible for most hot Jupiters, then all three subpopulations would have similar characteristic mean ages. If tidal evolution is efficient, then the inside-peak subpopulation will lose its oldest members and will therefore have a younger characteristic mean age; the other two subpopulations would be much less affected. If superimposed on an early-time population is a larger population of hot Jupiters formed via a late-time mechanism like high-eccentricity migration, then the preference for high-eccentricity migration to populate the orbital pe-

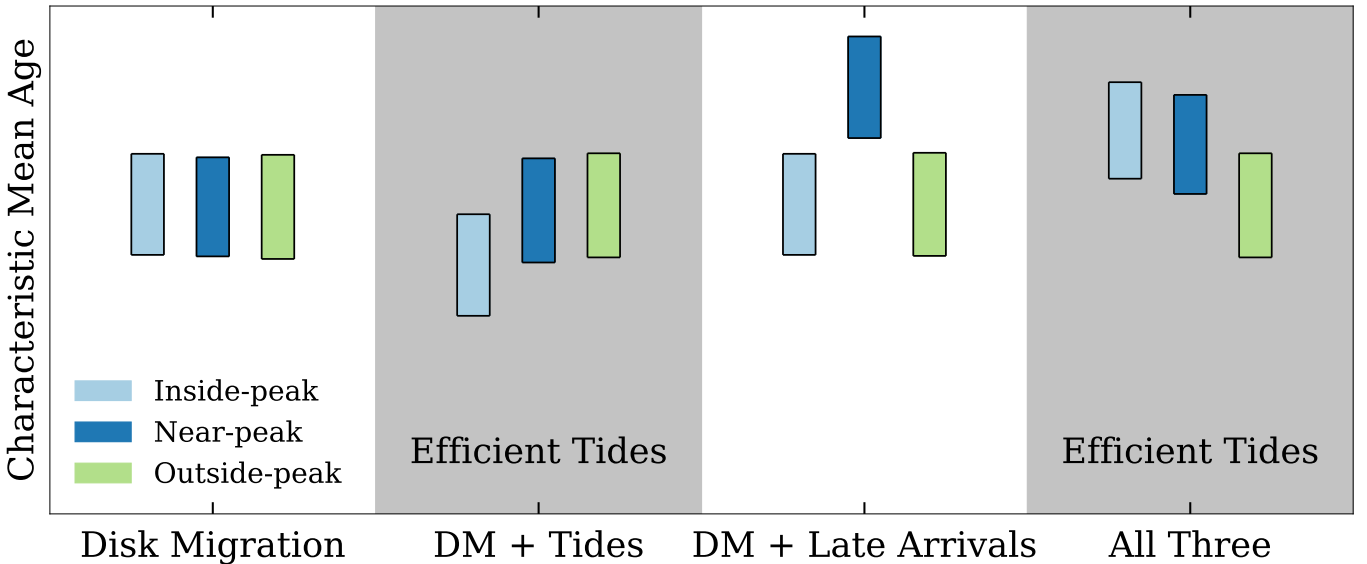


Figure 1. Cartoon of the characteristic mean ages expected for four different hot Jupiter formation scenarios: disk migration, disk migration plus tidal evolution, disk migration plus a late-time peak-populating mechanism, and disk migration plus a late-time peak-populating mechanism both affected by tidal evolution. The light blue, dark blue, and light green rectangles correspond to the inside-, near-, and outside-peak subpopulations, while we indicate with gray shading the scenarios for which tidal dissipation is important. In the two scenarios on the left, hot Jupiters form almost entirely from an early-time process that results in an approximately uniform distribution in orbital period (e.g., disk migration). In the two scenarios on the right, however, a large fraction of hot Jupiters form via a late-time process that results in a peaked orbital period distribution (e.g., high-eccentricity migration). Each scenario results in different age orderings for the three subpopulations, so we argue that characteristic mean age measurements should differentiate between them.

riod peak would result in an older near-peak subpopulation. If both early- and late-time mechanisms operate and tidal evolution is efficient, then the inside-peak subpopulation would be replenished by the older near-peak subpopulation, thereby increasing its characteristic mean age. At the same time, because the outside-peak subpopulation would have mostly formed via the early-time mechanism and be largely unaffected by tides, it would have the youngest characteristic mean age.

In this article we execute the test described in the preceding paragraph. We assemble our solar neighborhood subgiant sample and hot Jupiter subpopulations in Section 2. We then calibrate the age–velocity dispersion relation, calculate the subpopulations’ velocity dispersions, and obtain characteristic mean ages for each subpopulation in Section 3. We discuss the implications of our analyses in Section 4 and summarize our findings in Section 5.

2. DATA

New searches for hot Jupiters at longer orbital periods have enabled our investigation into the relative importance of hot Jupiter formation mechanisms. Most of these planets have been discovered by NASA’s Transiting Exoplanet Survey Satellite (TESS; [G. R. Ricker et al. 2014](#)), as its coverage of nearly the whole sky has

enabled a magnitude-limited search for transiting hot Jupiters out to $P \approx 10$ d and $T \approx 12$ (e.g., [S. W. Yee et al. 2022, 2023, 2025](#); [J. Schulte et al. 2024](#)). These new discoveries along with Gaia Data Release (DR) 3 astrometry and radial velocities² provide the data necessary for our experiment.

We select from the NASA Exoplanet Archive’s `pscomppars` table ([R. L. Akeson et al. 2013](#); [J. L. Christiansen et al. 2025](#); [NASA Exoplanet Archive 2025](#)) as of July 22, 2025 a sample of 503 hot Jupiters that meet the following criteria: $P_{\text{orb}} < 10$ d and $0.1 < M_p < 10 M_{\text{Jup}}$. We use the hot Jupiter orbital period and mass lower limit advocated by [J. T. Wright et al. \(2012\)](#) and the giant planet mass upper limit proposed by [K. C. Schlaufman \(2018\)](#). Due to Doppler surveyors’ historical avoidance of stars with observable emission in the cores of the Ca H and K lines, Doppler surveys have an intrinsic bias against young stars ([G. W. Marcy et al. 2005](#)). We select only transiting systems to avoid this age bias in our analysis sample. Our approach also re-

² For the details of Gaia DR3 and its data processing, see [Gaia Collaboration et al. \(2016, 2021, 2022, 2023\)](#), [C. Fabricius et al. \(2021\)](#), [L. Lindegren et al. \(2021a,b\)](#), [P. M. Marrese et al. \(2021, 2022\)](#), [M. Riello et al. \(2021\)](#), [N. Rowell et al. \(2021\)](#), [F. Torra et al. \(2021\)](#), and [C. Babusiaux et al. \(2023\)](#).

moves objects with only a minimum mass inference that may exceed our planet mass upper limit. Because the solar neighborhood age–velocity dispersion relation may not be the same as the age–velocity dispersion relation in the Kepler field (S. P. Schmidt et al. 2024), we exclude systems discovered by Kepler as well.

To calculate the Galactic velocity dispersions necessary to conduct our experiment, we require Gaia astrometry. We require Gaia DR3 `source_id` identifiers for every system in our analysis sample by first using the Gaia DR2 `source_id` identifier provided by the NASA Exoplanet Archive to find the DR3 `source_id` using the `dr2_neighbourhood` table. If a NASA Exoplanet Archive entry lacks a Gaia DR2 `source_id` but has a TESS Input Catalog (TIC; K. G. Stassun et al. 2019) ID, then we use the TIC ID to obtain a Gaia DR2 `source_id` and then follow the same procedure. If a NASA Exoplanet Archive entry lacks both a Gaia DR2 `source_id` and a TIC ID, then we use `astroquery` (A. Ginsburg et al. 2019) to query Simbad for the corresponding Gaia DR3 `source_id` corresponding to the system `hostname`.

We use the Gaia DR3 `source_id` identifiers and TOPCAT (M. B. Taylor 2005) to select equatorial positions, proper motions, parallaxes, and all covariances between these parameters for our analysis sample. We additionally collect radial velocities and associated uncertainties (D. Katz et al. 2023). To ensure high-quality Galactic UVW velocity measurements, we follow J. H. Hamer & K. C. Schlaufman (2024) and S. P. Schmidt et al. (2024) in requiring that `parallax_over_error` > 10 , `rv_nb_transits` > 10 , and `rv_expected_sig_to_noise` > 5 . To avoid unresolved binaries, we also require `ruwe` < 1.4 (C. Ziegler et al. 2020). We also collect the astrometric solution data necessary to correct for parallax zero-point offsets.

We supplement the radial velocities for our hot Jupiter sample by obtaining Apache Point Observatory Galactic Evolution Experiment (APOGEE; S. R. Majewski et al. 2017) heliocentric radial velocities and their associated uncertainties. This data was derived from spectra that were gathered during the third and fourth phases of the Sloan Digital Sky Survey (SDSS; D. J. Eisenstein et al. 2011; M. R. Blanton et al. 2017) as part of APOGEE. These spectra were collected with the APOGEE spectrographs (G. Zasowski et al. 2013, 2017; J. C. Wilson et al. 2019; R. L. Beaton et al. 2021; F. A. Santana et al. 2021) on the New Mexico State University 1-m Telescope (J. A. Holtzman et al. 2010) and the Sloan Foundation 2.5-m Telescope (J. E. Gunn et al. 2006). As part of SDSS DR 17 (Abdurro'uf et al. 2022), these spectra were reduced and analyzed with the APOGEE Stel-

lar Parameter and Chemical Abundance Pipeline (AS-PCAP; C. Allende Prieto et al. 2006; J. A. Holtzman et al. 2015; D. L. Nidever et al. 2015; A. E. García Pérez et al. 2016) using an H -band line list, MARCS model atmospheres, and model-fitting tools optimized for the APOGEE effort (R. Alvarez & B. Plez 1998; B. Gustafsson et al. 2008; I. Hubeny & T. Lanz 2011; B. Plez 2012; V. V. Smith et al. 2013, 2021; K. Cunha et al. 2015; M. Shetrone et al. 2015; H. Jönsson et al. 2020). We prefer these radial velocities over Gaia DR3 radial velocities in situations where both are available. It is valid to include both APOGEE and Gaia DR3 radial velocities due to their consistent zero points (e.g., S. P. Schmidt et al. 2024). We list the host Jupiter hosts in our analysis sample with their Gaia DR3 `source_id` identifiers, radial velocities, and radial velocity sources in Table 1.

Hot Jupiters tend to orbit metal-rich thin disk stars (e.g., N. C. Santos et al. 2004; D. A. Fischer & J. Valenti 2005). To ensure that our analysis sample is not contaminated by the thick disk, we calculate the maximum height above the mid plane z_{\max} for each system in our analysis sample. We integrate each star’s Galactic orbit from its position, parallax, proper motions, and radial velocity using the `gala` Python package (A. M. Price-Whelan 2017). Regardless of our assumption about the Galaxy’s gravitational potential used to integrate these orbits (e.g., variations on those presented by J. Bovy 2015), we find that no more than 10 hot Jupiter systems have a z_{\max} greater than 1 kpc, a potential indicator for thick disk membership.³ We therefore conclude that no more than 2% of our sample is in the high-velocity tail of the solar neighborhood velocity distribution.

To calibrate the solar neighborhood age–velocity dispersion relation, we follow the same procedure described above for the sample of subgiants with accurate, precise, and physically self-consistent age inferences presented in D. M. Nataf et al. (2024). As small differences in mass result in large differences in observed luminosity for stars transitioning from core to shell hydrogen fusion, subgiants represent the optimal stage of stellar evolution for age inference. D. M. Nataf et al. (2024) used MESA Isochrones and Stellar Tracks (MIST; B. Paxton et al. 2011, 2013, 2018, 2019; A. S. Jermyn et al. 2023; A. Dotter 2016; J. Choi et al. 2016) models and the `isochrones` Python package to infer fundamental and photospheric stellar parameters for 401,821 stars by fitting the MIST models to precise zero point-corrected Gaia DR3 parallaxes, multi-wavelength photometry, and extinction measurements from 3D reddening maps. The D. M.

³ We note that one system, the metal-poor WASP-183 system, has a particularly dynamically warm orbit.

Table 1. Hot Jupiter System Samples

System Name	Gaia DR3 <code>source_id</code>	RV (km s ⁻¹)	RV Source	Subpopulation
K2-77	37619725922094336	7.90 ± 0.03	APOGEE	Outside-peak
HD 285507	45159901786885632	38.02 ± 0.17	Gaia	Outside-peak
K2-87	47908509057301120	16.54 ± 0.02	APOGEE	Outside-peak
V1298 Tau	51886335968692480	15.62 ± 0.06	APOGEE	Outside-peak
TOI-5344	52359538285081728	45.00 ± 2.63	Gaia	Near-peak
K2-30	61607255708760960	36.18 ± 0.04	APOGEE	Near-peak
HAT-P-25	111322601672419712	-13.72 ± 1.06	Gaia	Near-peak
HAT-P-52	128623485853170432	60.92 ± 2.93	Gaia	Inside-peak
V830 Tau	147831571737487488	18.00 ± 0.05	APOGEE	Outside-peak
K2-29	150054788545735424	32.77 ± 0.48	Gaia	Inside-peak

NOTE—This table sorted by Gaia DR3 `source_id` and is published in its entirety in machine-readable format.

[Nataf et al. \(2024\)](#) catalog reports typical random uncertainties on age of $\sigma_\tau \approx 8\%$ and has been extensively validated with other catalogs of subgiant parameters. To enable a consistent comparison between the calibrated age–velocity dispersion relation and our hot Jupiter subpopulations’ velocity dispersions, we next remove all subgiants from this sample with $z_{\max} > 0.4$ kpc. This results in 88366 subgiants that pass all data quality cuts and have kinematics suggestive of thin disk membership.

3. ANALYSIS

To execute our experiment, we must divide our sample into inside-peak, near-peak, and outside-peak hot Jupiter subpopulations. While this subdivision could be made in several observable or inferable properties like orbital period P_{orb} , semimajor axis a , or scaled semimajor axis a/R_* , we favor and therefore use P_{orb} to subdivide the hot Jupiter sample because, unlike a and a/R_* , P_{orb} is directly observable from the light curves of all transiting exoplanet systems. Like all samples of transit-discovered exoplanets, our transiting hot Jupiter sample is biased as a consequence of the probability of transit:

$$P(\text{transit}) \propto \left(\frac{a}{R_*} \right)^{-1}, \quad (1)$$

where a/R_* is the scaled semimajor axis of the star–planet system. To address this bias, we therefore calculate the debiased median orbital period using the reported scaled semimajor axes from the NASA Exoplanet Archive as weights. We define the resulting orbital period $P_{\text{orb}} = 3.92$ d as the debiased peak of our analysis sample. To divide our analysis sample into the subpopulations described above, we first create the near-peak subpopulation by selecting one third of the analysis sample with orbital periods closest to the debiased peak. The resulting upper and lower orbital pe-

riod limits for this subpopulation are at 3.259 and 4.545 d. Our inferred debiased orbital period peak is consistent with the hot Jupiter occurrence peak observed by [A. Santerne et al. \(2016\)](#) among confirmed Kepler-discovered giant planets. We next place all hot Jupiters with $P_{\text{orb}} < 3.259$ d into the inside-peak subpopulation and likewise place all hot Jupiters with $P_{\text{orb}} > 4.545$ into the outside-peak subpopulation. We list the subpopulation membership of the systems in our analysis sample in Table 1.

It is well known that the occurrence of hot Jupiters increases strongly with host star metallicity ([N. C. Santos et al. 2004](#); [D. A. Fischer & J. Valenti 2005](#)). For that reason, a possible dependence of the solar neighborhood age–velocity dispersion relation on metallicity could bias the characteristic mean ages we infer for our analysis sample. To investigate this possibility, we divide our subgiant sample into four equal-size bins in metallicity: $-2.21 < [\text{Fe}/\text{H}] < -0.13$, $-0.13 < [\text{Fe}/\text{H}] < +0.06$, $+0.06 < [\text{Fe}/\text{H}] < +0.24$, and $+0.24 < [\text{Fe}/\text{H}] < +0.59$. Using a window size of 3000, we follow the methodology of [S. P. Schmidt et al. \(2024\)](#) to construct age–velocity dispersion relations for each metallicity bin. We show the results of these calculations in Figure 2. In the interval $2 \text{ Gyr} < \tau < 4 \text{ Gyr}$, appropriate for our subsequent analyses, the age–velocity dispersion relation is independent of metallicity. Though we will restrict our subgiant sample to a similar metallicity range to that spanned by our hot Jupiter sample for the calibration of our age–velocity dispersion relation, the effect of metallicity on this calibration is negligible.

We use the `pyia` Python package ([A. Price-Whelan 2018](#)) to convert equatorial coordinates, proper motions, parallaxes, and radial velocities into Galactic *UVW* space velocities. As has been the case with our previous kinematic analyses, the individual radial veloc-

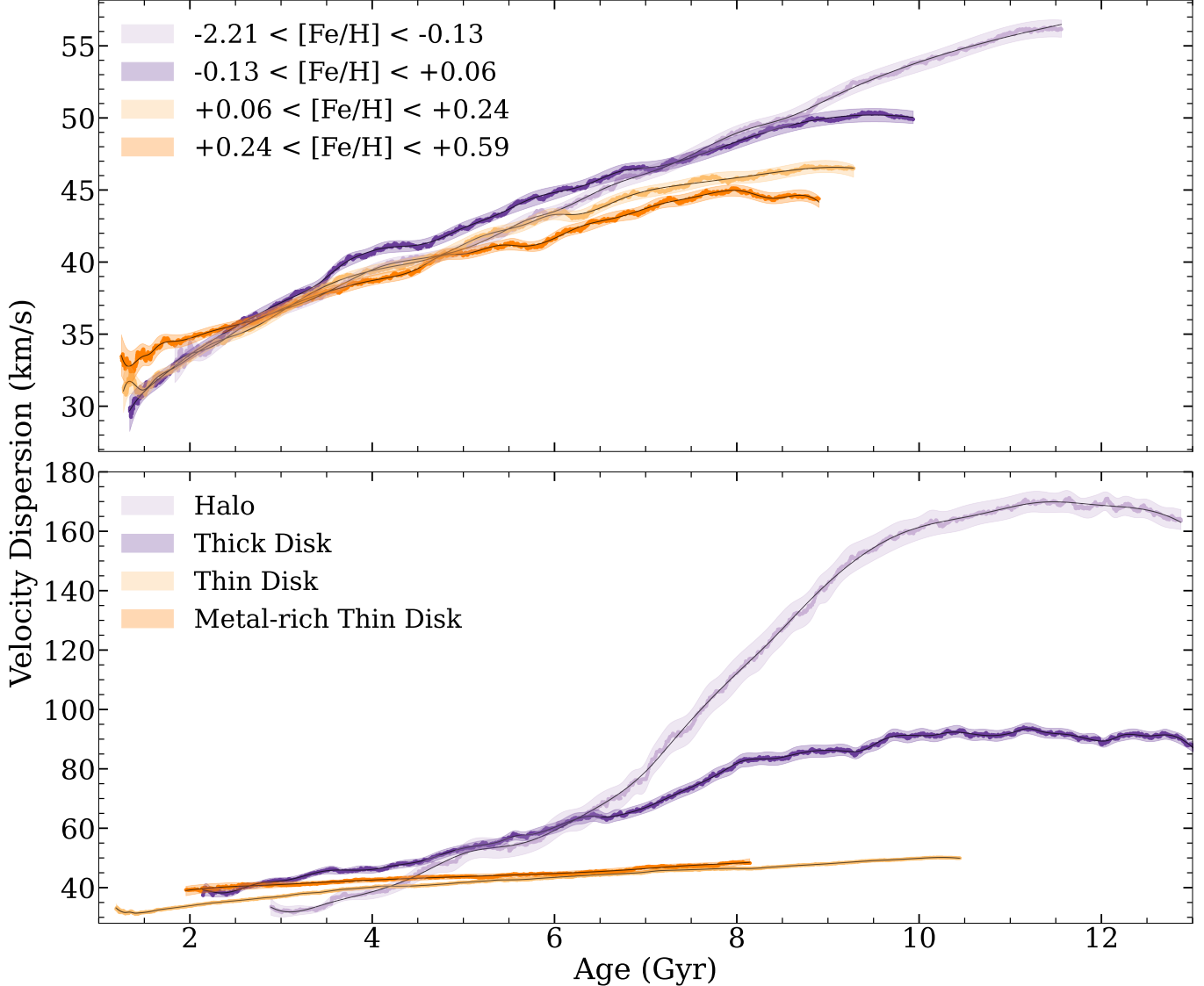


Figure 2. Solar neighborhood age–velocity dispersion relations as a function of metallicity. We subdivide the subgiant sample presented in D. M. Nataf et al. (2024) into four equal-size metallicity bins. We then order each subsample in age and calculate velocity dispersion in consecutive windows of 3000 stars. We plot the result of these calculations as overlapping colored points: light purple for the first quartile, dark purple for the second quartile, light orange for the third quartile, and dark orange for the fourth quartile. We plot as solid colored lines a smoothing spline of the respective data and as transparent polygons the 16th/84th interquartile ranges of the subsample’s velocity dispersion distribution suggested by bootstrap resampling. Though they exhibit noticeable differences in velocity dispersion at older ages, there is no significant metallicity dependence on velocity dispersion between 2 and 4 Gyr, the characteristic mean ages of our hot Jupiter subpopulations.

ity measurement uncertainties are an order of magnitude smaller than our velocity dispersion measurements, so our analyses are not limited by radial velocity precision. Prior to calculation of velocities, we use the `gaiadr3_zeropoint` Python package to correct each star’s parallax measurement (L. Lindegren et al. 2021a). We use a Monte Carlo simulation in which `pyia` randomly samples from the Gaia DR3 five-parameter astrometric solution respecting each solution’s covariance. It also independently randomly samples radial velocities

from a normal distribution with mean and variance as reported in each radial velocity source. We sample 100 realizations from each star’s astrometric uncertainty distributions in position, proper motion, parallax, and radial velocity using `pyia`. We then calculate the velocity dispersion σ of each sample

$$\sigma = \frac{1}{N} \sum_{i=1}^N [(U_i - \bar{U})^2 + (V_i - \bar{V})^2 + (W_i - \bar{W})^2]^{1/2}, \quad (2)$$

to construct an ensemble of samples of the entire populations' velocity dispersions. As was also the case in our previous velocity dispersion analyses (J. H. Hamer & K. C. Schlaufman 2019, 2020, 2022, 2024; S. P. Schmidt et al. 2024), \bar{U} , \bar{V} , and \bar{W} are the median U , V , and W velocities of the sample under consideration.

We use the same procedure to calculate UVW velocities for our sample of subgiants. According to the NASA Exoplanet Archive the interval between the 16th and 84th quantiles of our hot Jupiter sample's host stars metallicity distribution is $(-0.06, 0.36)$. To generate our calibrated age–velocity dispersion relation appropriate for comparison to our analysis sample, we therefore select subgiants with 1σ uncertainties in $[\text{Fe}/\text{H}]$ that overlap with this interval. This reduces our sample to 47390 subgiants. We next sort this metallicity-matched subgiant sample by age and calculate the mean age and velocity dispersion in a moving window sample of 5000 subgiants. We choose a window of 5000 to balance time resolution and velocity dispersion precision. This window is much larger than the window we use in S. P. Schmidt et al. (2024), as our metallicity-matched subgiant sample is more than an order of magnitude larger. We then advance the window by one star and then repeat this procedure until we cover the entire age range of our subgiant sample. For each 5000-star window, we sample with replacement within the window 150 bootstrap resamples of 5000 stars and calculate the velocity dispersion of each sample. We report in Table 2 the 16th, 50th, and 84th quantiles of the resulting velocity dispersion distributions. In parallel, we calculate the average age of the 5000 stars in each window. At the youngest ages, we use a reduced window size to maximize age resolution. We follow the same procedure described above, but we start each window with the youngest star and sequentially increase the window width from 150 to 5000 as the window advances. In contrast to previous studies of the relationship between age and velocity dispersion in the solar neighborhood (e.g., M. Aumer & J. J. Binney 2009; D.-C. Chen et al. 2021), our nonparametric approach does not assume or fit any functional form to the relationship. We use univariate smoothing splines to smooth the curves connecting the 16th, 50th, and 84th quantiles of the velocity dispersion distributions in each window, and we plot this smoothed age–velocity dispersion relation in Figure 3.

We next use this age–velocity dispersion relation to calculate velocity dispersion-based characteristic mean ages for our hot Jupiter subpopulations represented in Table 1. As in S. P. Schmidt et al. (2024), we infer lower and upper limits for these characteristic mean ages by identifying the range over which our inferred planet pop-

ulation mean velocity dispersions overlap with the 1σ range of the metallicity-constrained solar neighborhood age–velocity dispersion relation. We argue that this approach to age inferences is closest to the data itself. Conversely, other approaches that have assumed parametric relationships between age and velocity dispersion must account for random uncertainties in both their velocity dispersion measurements and the parameters of their parametric models like power law exponents (e.g., D.-C. Chen et al. 2021). We find that the characteristic mean age ranges for our inside-peak, near-peak, and outside-peak subpopulations are $3.16 \text{ Gyr} < \tau < 3.30 \text{ Gyr}$, $3.11 \text{ Gyr} < \tau < 3.27 \text{ Gyr}$, and $2.20 \text{ Gyr} < \tau < 2.36 \text{ Gyr}$. We show these ranges in Figure 4.

We find that the characteristic mean age of the outside-peak subpopulation is about 750 Myr younger than the near-peak and inside-peak subpopulations. In addition, the inside-peak subpopulation is slightly older than the near-peak subpopulation. This ordering supports the fourth scenario shown in Figure 1 and indicates that the formation and evolution of hot Jupiters can be attributed to meaningful contributions from an early-time, uniformly-distributing mechanism, a late-time, peak-populating mechanism, and tidal evolution.

Some potential observational biases could produce our observed age offset. As a system's transit probability is approximately the inverse of its scaled semimajor axis, hot Jupiters around more massive and therefore younger and larger host stars would be more likely to transit. However, the same is also true for hot Jupiters around older stars due to the radius expansion stars experience as they evolve on the main sequence.

To assess the age bias incurred by these competing effects, we construct a synthetic solar neighborhood sample of hot Jupiter host stars starting from Gaia DR3's `gaia_universe_model` data product. We select dwarf stars with $\log g > 3.75$ and $G < 12$ as an approximate limit for a “complete” magnitude-limited hot Jupiter population (S. W. Yee et al. 2021). To match the metallicity of this synthetic sample to our analysis sample, we also restrict it to $-0.06 < [\text{Fe}/\text{H}] < 0.36$. Because we are only concerned with age differences resulting from the bias described above and not the overall occurrence of hot Jupiters, to maximize the precision of our bias quantification it is acceptable to assume that all stars in our synthetic sample host hot Jupiters. We then perform a Gaussian kernel density estimation on our debiased hot Jupiter period distribution to generate orbital periods for each synthetic system. We next assume an isotropic inclination distribution and select transiting systems following Equation (1) of R. L. Gilliland et al. (2000). Dividing each realization's entire population into inside-

Table 2. Solar Neighborhood Age–Velocity Dispersion Relation for Hot Jupiter Hosts

Window	Average Age	Lower Uncertainty	Velocity Dispersion	Upper Uncertainty
	(Gyr)	(km s ⁻¹)	(km s ⁻¹)	(km s ⁻¹)
	1.21211	1.28785	32.12854	1.23260
	1.21268	1.33804	32.11174	1.29713
	1.21324	1.33564	32.05038	1.40146
	1.21379	1.26139	31.95224	1.20396
	1.21435	1.02253	31.86713	1.00291
	1.21490	1.17319	31.92756	1.26564
	1.21544	1.15702	31.98542	1.23763
	1.21597	1.33164	31.83756	1.40988
	1.21651	1.05254	31.83700	1.07099
	1.21704	1.25875	31.84092	1.38797

NOTE—This table is ordered by average age in ascending order and is published in its entirety in machine-readable format. This age–velocity dispersion relation uses subgiants in a metallicity range restricted to reflect that of hot Jupiter hosts. Lower uncertainty refers to the difference between the 50th and 16th quantiles, and the upper uncertainty refers to the difference between the 84th and 50th quantiles.

peak, near-peak, and outside-peak subpopulations, we calculate the median age of each subpopulation. Finally, we create an ensemble of age differences between the near-peak and outside-peak subpopulations to assess a potential age bias. We find that the $1-\sigma$ range of the age offset distribution is consistent with zero whether or not we apply a metallicity cut. The same is true when we relax the apparent G magnitude limit to $G < 14$ regardless of metallicity. Likewise, there is no change if we exclude stars close to the ecliptic plane that have been less intensively studied by TESS than stars at the ecliptic poles. As a result, we can conclude that any age differences we observe are caused by the time evolution of hot Jupiter systems. We note that there is no relationship between age and metallicity in the thin disk of the Milky Way (e.g., M. Xiang & H.-W. Rix 2022; D. M. Nataf et al. 2024), so there is no need to consider biases that might result from a relationship between age and metallicity in our sample.

4. DISCUSSION

In our solar neighborhood hot Jupiter analysis sample, we find that the outside-peak subpopulation has a characteristic mean age in the range $2.20 \text{ Gyr} \lesssim \tau \lesssim 2.36 \text{ Gyr}$. On the other hand, we find that the near- and inside-peak subpopulations have characteristic mean ages in the ranges $3.11 \text{ Gyr} \lesssim \tau \lesssim 3.27 \text{ Gyr}$ and $3.16 \text{ Gyr} \lesssim \tau \lesssim 3.30 \text{ Gyr}$. We emphasize that the characteristic mean ages we quote are statistical measurements of population mean ages, and that individual systems may be older or younger than their subpopulation’s characteristic mean age.

We highlight the importance of analyzing transit-discovered systems separately from Doppler-discovered systems because of the selection effects that shape both samples. In particular, Doppler surveyors tend to avoid young stars because young stars have large radial velocity jitters that make detection and characterization of small Doppler signals difficult. While the transit technique is also biased against young and therefore highly photometrically variable stars, this effect is less severe. To quantify these effects in terms of characteristic mean age offsets, we calculate the velocity dispersions of three additional samples of giant exoplanets with $P_{\text{orb}} > 10 \text{ d}$ and plot these results in Figure 5: (1) systems discovered via the Doppler technique, (2) systems discovered via the transit technique, and (3) the union of (1) and (2). As most giant planets with $P_{\text{orb}} > 10 \text{ d}$ have been discovered via the Doppler technique, sample (3) is dominated by older, low-jitter stars and has a velocity dispersion similar to sample (1). As expected, those samples’ velocity dispersions are much warmer than that of sample (2). We are therefore justified in focusing our analysis of hot Jupiter subpopulations on transit discoveries alone.

While we have established in Section 3 that multiple mechanisms contribute to the hot Jupiter population, those analyses alone do not constrain the relative contributions from each mechanism. To quantify these proportions, we develop a parametric forward model for the formation and evolution of the hot Jupiter subpopulations with these proportions as independent variables. We model the hot Jupiter population with three formation mechanisms: (1) an early-time, uniformly-distributing mechanism, (2) an early-

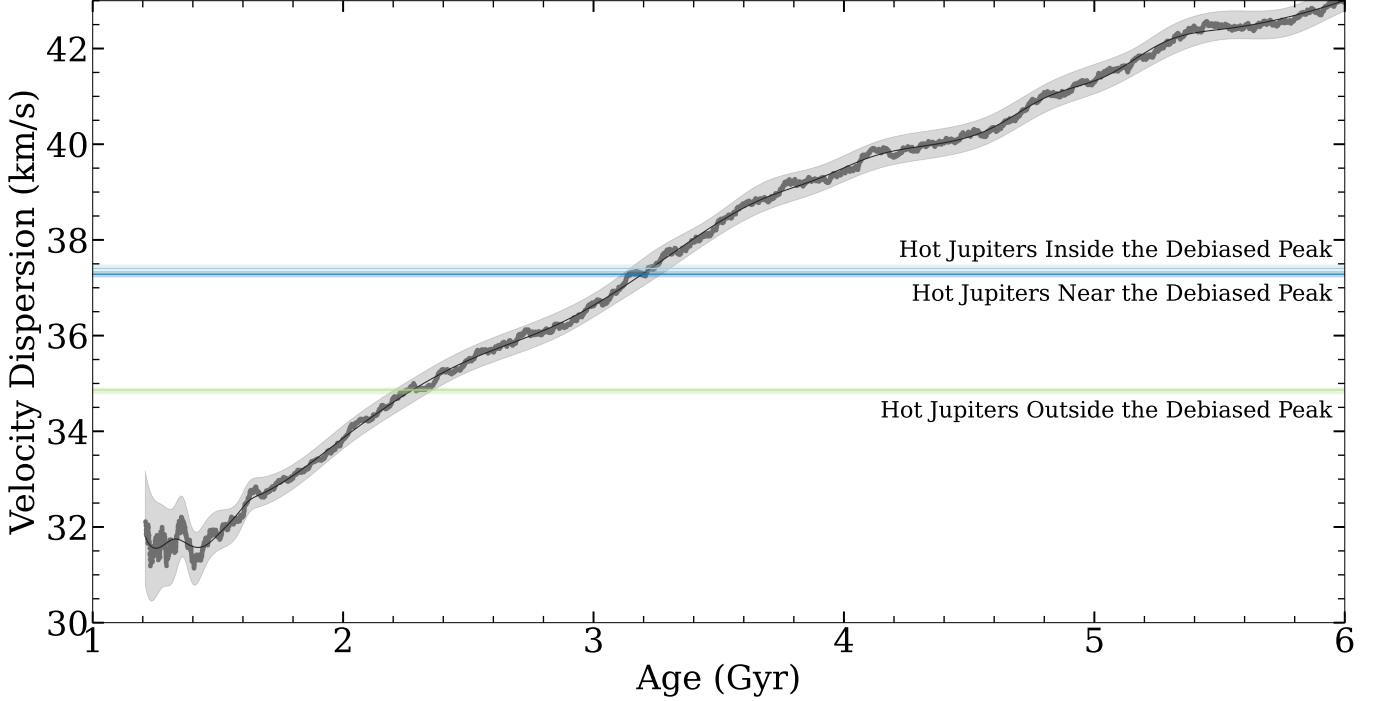


Figure 3. Solar neighborhood age–velocity dispersion relation for the metallicity interval $-0.06 < [\text{Fe}/\text{H}] < +0.36$ appropriate for hot Jupiter hosts as explained in Section 3. We follow the same procedure we use to generate Figure 2 and plot as the black line the resulting smoothed age–velocity dispersion relation and as the gray polygon its 16th/84th interquartile range. We calculate the debiased median period of the hot Jupiter period distribution by weighting hot Jupiter systems’ orbital periods by their scaled semimajor axes a/R_* to account for the observational biases present in the transit technique that has discovered most hot Jupiters. The near-peak subpopulation comprises one third of the overall sample with orbital periods closest to this debiased median period. We then create two additional subpopulations: one inside the debiased peak with orbital periods shorter than the near-peak subpopulation and one outside the debiased peak with orbital periods longer than the near-peak subpopulation. We plot as light blue, dark blue, and light green horizontal lines the velocity dispersions of the inside-, near-, and outside-peak hot Jupiter subpopulations. The inside-peak and near-peak subpopulations have characteristic mean ages $\tau \approx 3.2$ Gyr, with the inside-peak subpopulation slightly older than the near-peak subpopulation. On the other hand, the outside-peak subpopulation has a characteristic mean age $\tau \approx 2.3$ Gyr. The distinctly younger age of the outside-peak subpopulation relative to the inside- and near-peak subpopulations supports the fourth scenario in Figure 1. In that scenario, the combination of (1) an early-time formation channel that produces a uniform period distribution, (2) a late-time formation channel that produces a peaked period distribution, and (3) subsequent tidal evolution have all contributed to the formation and evolution of the hot Jupiter population.

time, peak-populating mechanism, and (3) a late-time, peak-populating mechanism. To initialize our host star and hot Jupiter masses, we self-consistently calculate host star masses for all of the hot Jupiters in the NASA Exoplanet Archive and use the system’s observed inclinations, Doppler semiamplitudes, and eccentricities to calculate planet masses. We initialize our orbital periods in two different ways. We first initialize the early-time, uniform component by distributing some fraction f_{EU} of hot Jupiters at initial orbital periods distributed as $\mathcal{U}(1, 10)$ d. We next initialize both the early-time and late-time, peak-populating components with initial orbital periods distributed as $\mathcal{N}(4, 0.5^2)$ d and proportions f_{EP} and f_{LP} . We require $f_{\text{EU}} + f_{\text{EP}} + f_{\text{LP}} = 1$, so only two of these three variables are independent (f_{LP} and f_{EP} in our forward model).

Because newly-formed giant planets may have nonzero eccentricities, for the early-time, uniformly-distributing mechanism we use a $\text{Beta}(0.867, 3.03)$ eccentricity distribution following D. M. Kipping (2013). For the both the early-time and late-time peak-populating mechanisms we use the inner planet eccentricity distribution observed in the Mass Distribution 3 simulation from S. Chatterjee et al. (2008) planet–planet scattering simulations. Though core mass has little effect on the resulting eccentricity distribution predicted from planet–planet scattering, we select this set of simulations as it permits core masses larger than $10 M_{\oplus}$ that have been inferred for several planets (e.g., P. B. Buhler et al. 2016; L. Welbanks et al. 2024; D. K. Sing et al. 2024). We approximate the S. Chatterjee et al. (2008) eccentricity distribution as $\text{Beta}(2.67, 5.67)$ and use it to initialize ec-

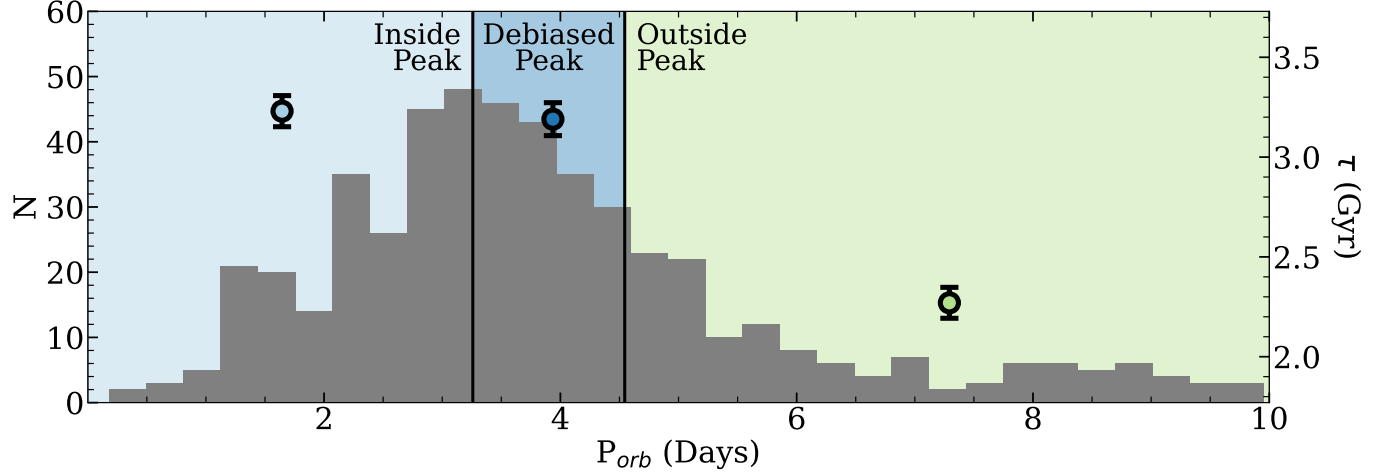


Figure 4. Illustration of the three hot Jupiter subpopulations and their characteristic mean ages. We plot as the gray histogram the orbital period distribution of our solar neighborhood transiting hot Jupiter sample. We mark with vertical black lines the boundaries of the three subpopulations we have identified and shade the inside-, near-, and outside-peak subpopulations in light blue, dark blue, and light green. We plot the characteristic mean age ranges as the black error bars in each region. We find that the inside-peak subpopulation is older, but still statistically consistent with, the characteristic mean age of the near-peak subpopulation. In contrast, the outside-peak subpopulation is younger than both shorter-period subpopulations. We argue that this ordering in age plus the statistically younger characteristic mean age of the outside-peak subpopulation is best explained by a late-time, peak-populating formation mechanism that is responsible for placing most hot Jupiters near and inside the debiased orbital period peak. Subsequent tidal evolution would then move some of these hot Jupiters to shorter orbital periods over billions of years.

centricities for both peak-populating mechanisms. For both peak-populating mechanisms, we additionally increase the initial separations of these planets by a factor of $(1 - e^2)^{-1}$ such that they start out still undergoing circularization before arriving (approximately, assuming conservation of angular momentum) at an orbital period corresponding to the selected orbital period distributed as $\mathcal{N}(4, 0.5^2)$ d. We initialize host stellar obliquities for both the early-time and late-time peak-populating mechanisms with a Beta(1.42, 12.8) distribution multiplied by a scaling factor of 180 degrees to approximate the [S. Chatterjee et al. \(2008\)](#) obliquity distribution.

To model the subsequent tidal evolution in our forward model, we use the best existing constraint on the giant planet specific tidal quality factor $Q'_p = 3.56 \times 10^5$ derived for Jupiter from observations of its Galilean satellites ([V. Lainey et al. 2009](#)). We use the tidal evolution model presented in [J. Leconte et al. \(2010\)](#) in combination with [L. Amard et al. \(2019\)](#) rotational stellar evolution models to account for tidal evolution. We interpolate the [L. Amard et al. \(2019\)](#) grid to obtain a rotational stellar evolution track for each system considered in our forward model. Because the specific tidal quality factors for main sequence dwarf stars are poorly constrained, we execute our forward model for four different values of Q'_* : $Q'_* = 10^{6.0}$, $Q'_* = 10^{6.5}$, $Q'_* = 10^{7.0}$, and $Q'_* = 10^{7.5}$.

As planetary systems are continuously being formed in the Milky Way's thin disk, we simulate approximately constant system formation up to the age of the solar neighborhood by uniformly distributing system formation times as $\mathcal{U}(0, \text{Min}(t_{\text{MS}}, 8))$ Gyr, where t_{MS} is the time at which the host star's surface gravity $\log g < 4.0$ (i.e., its main sequence lifetime). As there is no first principles reason to favor any particular value for the time between the early-time and late-time hot Jupiter formation mechanisms, we execute our forward model using a range of potential time lags. For the late-time hot Jupiter formation mechanism, we parameterize this time lag as the average time between system formation and the formation of the hot Jupiter, $\Delta\tau$. We first construct a sequence of values for $\Delta\tau$ from 500 Myr to 2.5 Gyr spaced by 250 Myr. Any smaller values of $\Delta\tau$ would be difficult to observationally distinguish, and any larger values of $\Delta\tau$ would be unphysical given our inferred subpopulation characteristic mean ages. For the early-time hot Jupiter formation mechanisms, we start tidal evolution 10 Myr after system formation corresponding to the dissipation of the parent protoplanetary disk. For hot Jupiters formed via the late-time, peak-populating mechanism with P_{orb} distributed as $\mathcal{N}(4, 0.5^2)$ d, we start tidal evolution after an additional period of time distributed as $\mathcal{N}(\Delta\tau, 0.5^2)$ Gyr. We illustrate several scenarios for individual hot Jupiter systems under these formation assumptions and $Q'_* = 10^7$ in Figure 6.

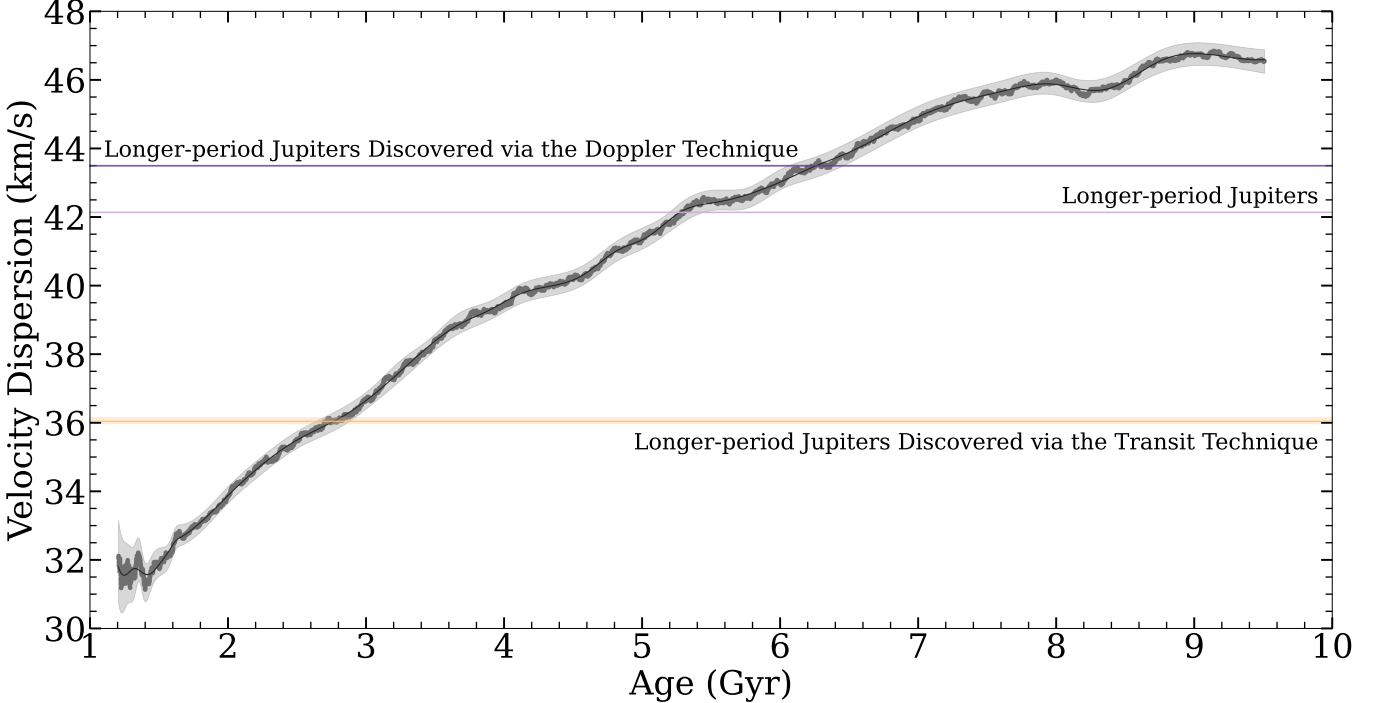


Figure 5. The same age–velocity dispersion relation as in Figure 3. To emphasize the effect of observational biases on the characteristic mean ages of exoplanet systems, we plot as horizontal lines the velocity dispersions of all known giant planet systems with orbital periods $P > 10$ d (light purple), the subset of these systems discovered via the Doppler technique (dark purple), and the subset of these systems discovered via the transit technique (orange). Because by itself the Doppler technique is only sensitive to long-period giant planets orbiting quiescent stars, Doppler surveyors have usually avoided stars with chromospheric emission indicative of youth. This bias against young stars in the population of Doppler-discovered exoplanet systems makes comparing the mean ages of the Doppler- and transit-discovered exoplanet populations challenging. We caution against combining populations of planets detected via more than one technique for system age-related analyses without first accounting for biases incurred by each detection method.

On each iteration of our 500-iteration Monte Carlo simulations, an initial hot Jupiter population of 500 systems is generated according to the parameters described above. It is then evolved to the present, eliminating systems where the planet is tidally disrupted and ignoring the few (if any) systems with orbital periods that increase beyond $P_{\text{orb}} > 10$ d. We split the surviving population into thirds by orbital period and calculate each subpopulation’s median age. Marginalizing over all 500 iterations, we calculate the 16th, 50th, and 84th quantiles of the resulting age distributions.

We plot the final outcome of our forward modeling in Figures 7 and 8. We find that $10^{6.5} \lesssim Q'_* \lesssim 10^7$, $0.4 \lesssim f_{\text{LP}} \lesssim 0.8$, and $\Delta\tau \gtrsim 1.5$ Gyr can quantitatively reproduce our observations that: (1) subpopulation age decreases with orbital period, (2) the outside-peak subpopulation is significantly younger than the near- and inside-peak subpopulations, (3) the characteristic mean age of the outside-peak subpopulation is at least 750 Myr younger than the near- and inside-peak subpopulations, and (4) the characteristic mean age of the inside-peak subpopulation is at most 200 Myr older than

the near-peak subpopulation. In other words, we find that at least 40% of hot Jupiters formed via a late-time, peak-populating mechanism with a characteristic time delay of more than 1.5 Gyr. Our conclusion that $0.4 \lesssim f_{\text{LP}} \lesssim 0.8$ is consistent with the [J. M. Jackson et al. \(2023\)](#) constraint that no more than 62% of hot Jupiters in the Kepler field were produced via high-eccentricity migration followed by tidal circularization. While we can only exclude values for Q'_* outside the interval $(10^6, 10^{7.5})$, we favor values in the interval $(10^{6.5}, 10^7)$ because they both produce forward models quantitatively consistent with our observations and are consistent with the [J. H. Hamer & K. C. Schlaufman \(2019\)](#) constraint $Q'_* \lesssim 10^7$. A broader range of parameters Q'_* , f_{LP} , and $\Delta\tau$ can qualitatively reproduce our observations that: (1) subpopulation age decreases with orbital period, and (2) the outside-peak subpopulation is significantly younger than the near- and inside-peak subpopulations. In this qualitative agreement case, only a minority of hot Jupiters can form via the early-time,

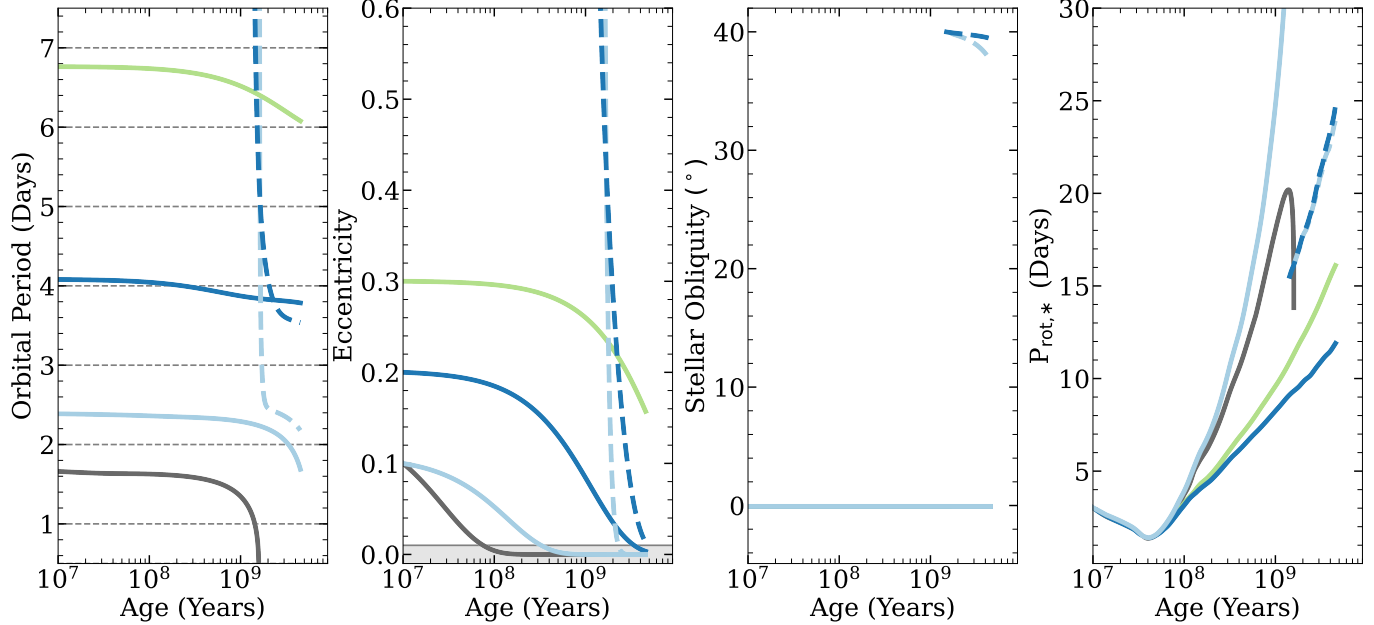


Figure 6. Six possible outcomes of tidal evolution in hot Jupiter systems according to the [J. Leconte et al. \(2010\)](#) model assuming the rotational stellar evolution models presented in [L. Amard et al. \(2019\)](#). We consider two scenarios for hot Jupiter formation: (1) four realizations of an early-arrival mechanism that produces a uniform orbital period distribution and (2) two realizations of a late-arrival mechanism that produces a peaked orbital period distribution. We plot as a function of system age colored lines corresponding to system orbital period P (left), eccentricity e (center left), stellar obliquity ψ (center right), and stellar rotation period $P_{\text{rot},*}$ (right). We indicate the four realizations of the early arrival scenario with solid lines and the two realizations of the late arrival scenario with dashed lines. Early-arriving hot Jupiter systems with small separations experience inspiral, while all hot Jupiter systems experience eccentricity damping to some extent. For hot Jupiter systems outside the debiased orbital period peak (light green), circularization to $e < 0.01$ as indicated by the gray rectangle typically takes longer than the current age of the system. Hot Jupiter systems near the debiased orbital period peak (dark blue) may circularize on a comparable timescale to the systems' ages, while early-arriving small-separation systems circularize quickly (light blue) and may be engulfed (gray). On the other hand, hot Jupiter systems formed via a late-time, peak-populating mechanism would be less evolved and still observable later in their host stars' main sequence lifetimes. We expect these late arrivals to have nonzero host star obliquities, while the host stars of hot Jupiters that have experienced significant inspiral should be rotating more quickly than stars of similar masses and ages.

uniformly-populating mechanism that we use to model disk migration or in situ formation.

While the near- and inside-peak subpopulations of the overall hot Jupiter population experience significant tidal inspiral during the main sequence lifetimes of their host stars, the outside-peak subpopulation is unaffected by inspiral in this time interval. Therefore, the outside-peak subpopulation is robust to tidal inspiral for the entire main sequence lifetimes of their host stars. It is this outside-peak subpopulation that was underrepresented in the [J. H. Hamer & K. C. Schlaufman \(2019\)](#) analysis that was dominated by ground-based transit discoveries that has since been observed as hot Jupiters orbiting evolved stars (e.g., [N. Saunders et al. 2022, 2025](#); [S. K. Grunblatt et al. 2022](#); [F. Pereira et al. 2024](#)). This reconciles the apparently conflicting claims of [J. H. Hamer & K. C. Schlaufman \(2019\)](#) and [S. K. Grunblatt et al. \(2023\)](#).

Our observed ages and population modeling imply that most of the hot Jupiters that exist near the debiased peak of the orbital period distribution formed in a different manner from those outside the debiased peak. The outside-peak hot Jupiter subpopulation therefore represents the inner edge of the aligned, disk migration/in situ formation-dominated regime that we expect to produce small host star obliquities. This expectation has been confirmed by Rossiter–McLaughlin measurements of longer-period giant planet systems⁴. Because the hot Jupiters in the outside-peak subpopulation take much longer than their current system ages to circular-

⁴ See, for example, [S. Wang et al. \(2021\)](#), [E. Knudstrup & S. H. Albrecht \(2022\)](#), [M. Rice et al. \(2022b\)](#), [J. Lubin et al. \(2023\)](#), [E. Sedaghati et al. \(2023\)](#), [J. Wright et al. \(2023\)](#), [J. I. Espinoza-Retamal et al. \(2023\)](#), [Q. Hu et al. \(2024\)](#), [X.-Y. Wang et al. \(2024\)](#), [A. Bieryla et al. \(2025\)](#), and [J. I. Espinoza-Retamal et al. \(2025\)](#).

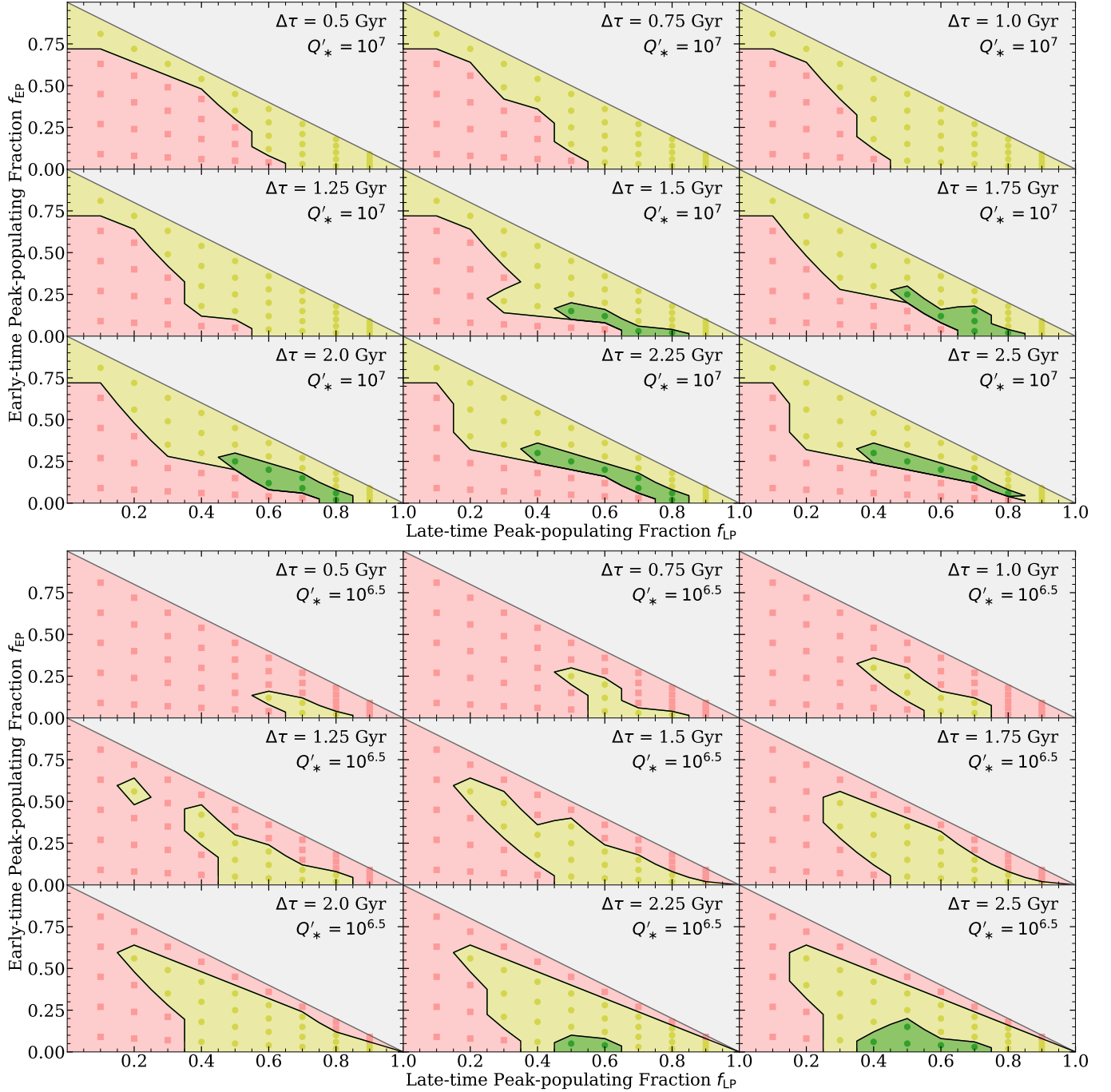


Figure 7. Outcome of our parametric forward model for the formation and evolution of the hot Jupiter population assuming stellar tidal quality factors $Q'_* = 10^7$ (top) and $Q'_* = 10^{6.5}$ (bottom). In each of the nine panels of each plot we vary four parameters in our forward model: (1) the fraction of the hot Jupiter population that formed via a late-time, peak-populating mechanism f_{LP} , (2) the fraction of the hot Jupiter population that formed via an early-time, uniformly-distributing mechanism f_{EU} , (3) the fraction of the hot Jupiter population that formed via an early-time, peak-populating mechanism f_{EP} , and (4) the average time between system formation and late-time mechanism occurrence for systems that formed via the late-time mechanism $\Delta\tau$. We require $f_{LP} + f_{EU} + f_{EP} = 1$. To populate each panel, for each point in (f_{LP}, f_{EU}, f_{EP}) space we execute a Monte Carlo simulation as described in Section 4. Because we find that the characteristic mean ages of our three hot Jupiter subpopulations decrease with orbital period, we plot in red regions of parameter space inconsistent with this ordering or with an outside-peak subpopulation not significantly younger than the near- and inside-peak subpopulations. In contrast, we plot in yellow and green regions of parameter space where both of these criteria are met. In green regions it is also true that the characteristic mean age of the outside-peak subpopulation is at least 750 Myr younger than the near- and inside-peak subpopulations and that the characteristic mean age of the inside-peak subpopulation is at most 200 Myr older than the near-peak subpopulation. We find $0.4 \lesssim f_{LP} \lesssim 0.8$, $\Delta\tau \gtrsim 1.5$ Gyr, and $10^{6.5} \lesssim Q'_* \lesssim 10^7$ best reproduce our observations, indicating that at least 40% hot Jupiters are late arrivals taking more than 1.5 Gyr to become hot Jupiters.

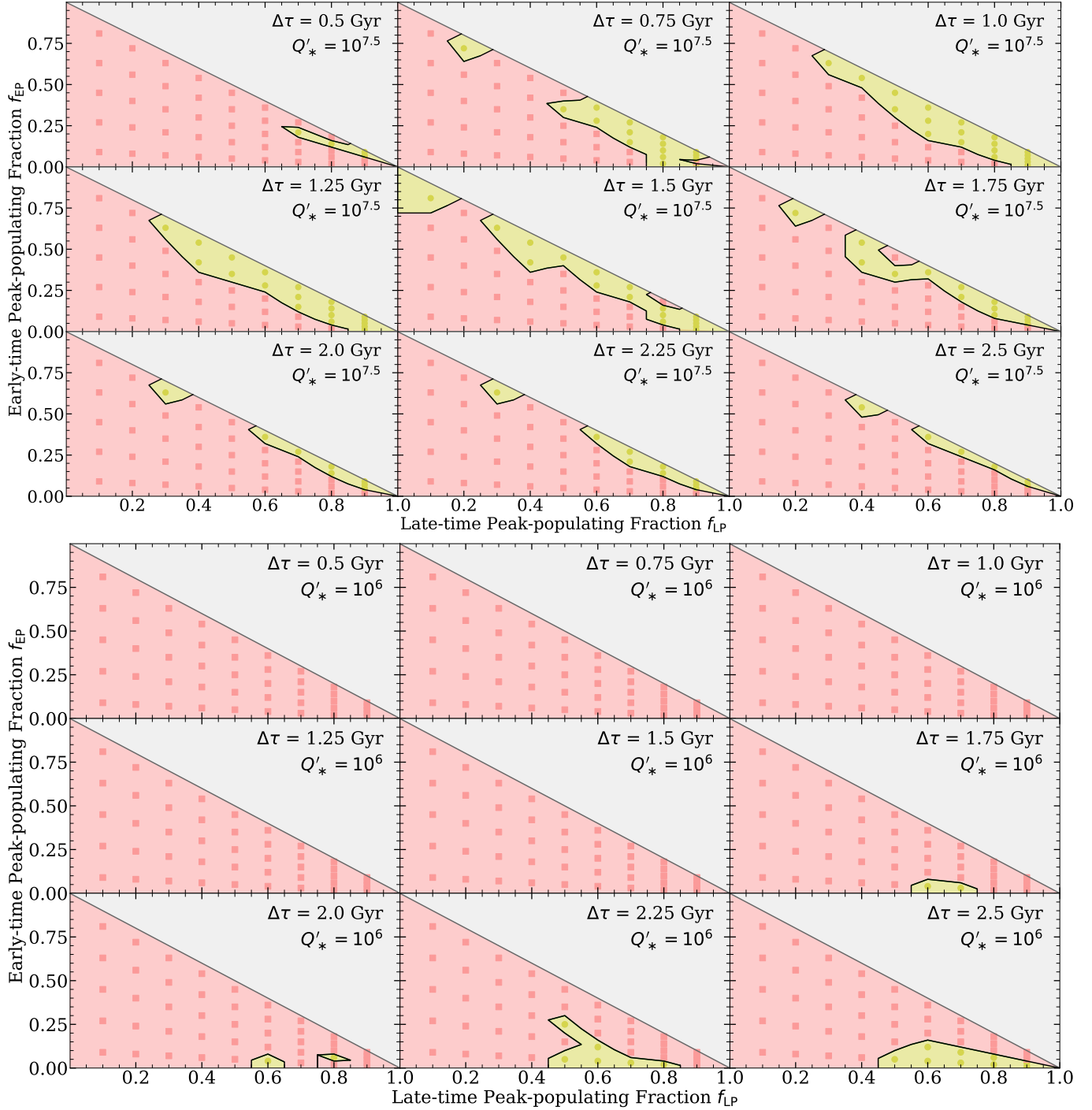


Figure 8. Outcome of our parametric forward model for the formation and evolution of the hot Jupiter population assuming stellar tidal quality factors $Q'_* = 10^{7.5}$ (top) and $Q'_* = 10^6$ (bottom) and therefore more/less dissipative host stars than presented in Figure 7. While $Q'_* = 10^6$ and $Q'_* = 10^{7.5}$ do not produce outcomes quantitatively consistent with our results, they do produce results qualitatively consistent with our conclusion that $\gtrsim 40\%$ of the hot Jupiter population are late arrivals with $\Delta\tau \approx 2$ Gyr. We therefore favor Q'_* values in the range $10^{6.5} \lesssim Q'_* \lesssim 10^7$ because those parameters result in quantitative agreement with our observations. Nevertheless, the range $10^6 \lesssim Q'_* \lesssim 10^{7.5}$ is qualitatively consistent with our observations.

ize and therefore exhibit nonzero eccentricities, our interpretation is also consistent with the observation that eccentric hot Jupiters' orbits do not exhibit the same obliquity-host star mass trend (M. Rice et al. 2022a) as hot Jupiters on circular orbits (K. C. Schlaufman 2010; J. N. Winn et al. 2010).

If our interpretation of our observations is correct, then the peak of the hot Jupiter orbital period distribution should be less prominent at ages $\tau \lesssim 1$ Gyr. We therefore predict that as the sample of hot Jupiters with system ages $\tau \lesssim 1$ Gyr grows, it should have a less pronounced peak in its orbital period distribution. We also predict that the occurrence of wide-separation giant planet, brown dwarf, or stellar companions should be higher for the near-peak subpopulation than the outside-peak subpopulation. We emphasize that these conclusions have been made possible as a result of TESS's many discoveries of hot Jupiters in the outside-peak subpopulation that were largely invisible to ground-based transit surveys. Therefore, studies of hot Jupiter demographics that were dominated by ground-based discoveries should be reevaluated in light of these new discoveries.

In addition to our prediction for the orbital period distribution of hot Jupiters orbiting stars younger than about 1 Gyr, we also expect an increased occurrence of additional wide-separation companions. In contrast to hot Jupiters outside the debiased peak of the orbital period distribution, hot Jupiters near the debiased orbital period peak could evince these additional companions (1) in Doppler data as additional Keplerian orbits or an increased occurrence of long-term trends, (2) in transit data as an increased occurrence of transit-timing variations, or (3) in astrometric data as additional Keplerian orbits or an increased occurrence of astrometric accelerations. We therefore advocate for long-term baseline monitoring of relatively recently discovered hot Jupiters that are part of the outside-peak subpopulation to build up the time baseline needed to evaluate these possibilities.

These interpretations of our observations could also explain in part the increased hot Jupiter occurrence in pure Doppler-based surveys for hot Jupiters (e.g., M. Mayor et al. 2011; J. T. Wright et al. 2012) in comparison to the diminished hot Jupiter occurrence in transit-based surveys (e.g., A. Santerne et al. 2012; F. Fressin et al. 2013; A. Santerne et al. 2016). While M. Moe & K. M. Kratter (2021) persuasively argued that a difference in the binarity of the Doppler- and transit-surveyed populations plays the primary role in this apparent occurrence difference, other factors may also contribute. If as suggested by Figure 5 Doppler-based surveys are

biased towards older stars, then more Doppler-searched systems would have had enough time for a hot Jupiter to form as described above than a similar sample of systems searched for transiting hot Jupiters. Indeed, Doppler surveyors preferentially target stars with Ca II H and K emission indicative of ages greater than 2 Gyr—exactly the time delay indicated by our forward model (e.g., G. W. Marcy et al. 2005).

If our interpretation of our observations is correct, then the age of the outside-peak subpopulation should be consistent with the age of a matched control sample of stars without observed hot Jupiters. The Kepler field is the ideal environment for this validation of our interpretation, as the sample of dwarf stars searched for transiting planets by Kepler is known. We conduct this test of our proposed scenario for the formation of the outside-peak subpopulation by comparing (1) the velocity dispersion of the host stars of the Kepler-discovered hot Jupiter sample's outside-peak subpopulation to (2) an ensemble of dwarf stars in the Kepler field searched for planets but without observed transiting hot Jupiters. Following the approach of J. H. Hamer & K. C. Schlaufman (2019), we match these samples in mass and metallicity using the T. A. Berger et al. (2020) catalog of stellar parameters and confirm that the velocity dispersion of the outside-peak subpopulation of the Kepler field's hot Jupiter population is indeed consistent with velocity dispersion distribution produced by control samples matched in mass and metallicity. We visualize the results of this test in Figure 9. This analysis further supports our conclusion that the hot Jupiters in the outside-peak subpopulation formed early and have not been substantially affected by tidal inspiral to the point of disruption by their host stars.

Finally, we note that many objects classified as hot Jupiters can retain the post-formation orbital eccentricities for many Gyr. Since obliquity damping generally takes longer than eccentricity damping, the same is also true for the stellar obliquities of hot Jupiter host stars. To demonstrate this, we calculate the eccentricity damping timescale for a range of hot Jupiter system initial semimajor axes and eccentricities. Assuming a median rotation L. Amard et al. (2019) $1 M_{\odot}$ stellar model with $Q'_* = 10^7$, the J. Leconte et al. (2010) tidal evolution model suggests that a significant fraction of hot Jupiters ($P_{\text{orb}} \gtrsim 4$ d and $e \lesssim 0.3$) will avoid orbit circularization and therefore obliquity damping on Gyr timescales (Figure 10). Our calculations show that studies of the post-formation eccentricities and obliquities of giant planets need not restrict their samples to $P_{\text{orb}} > 10$ d.

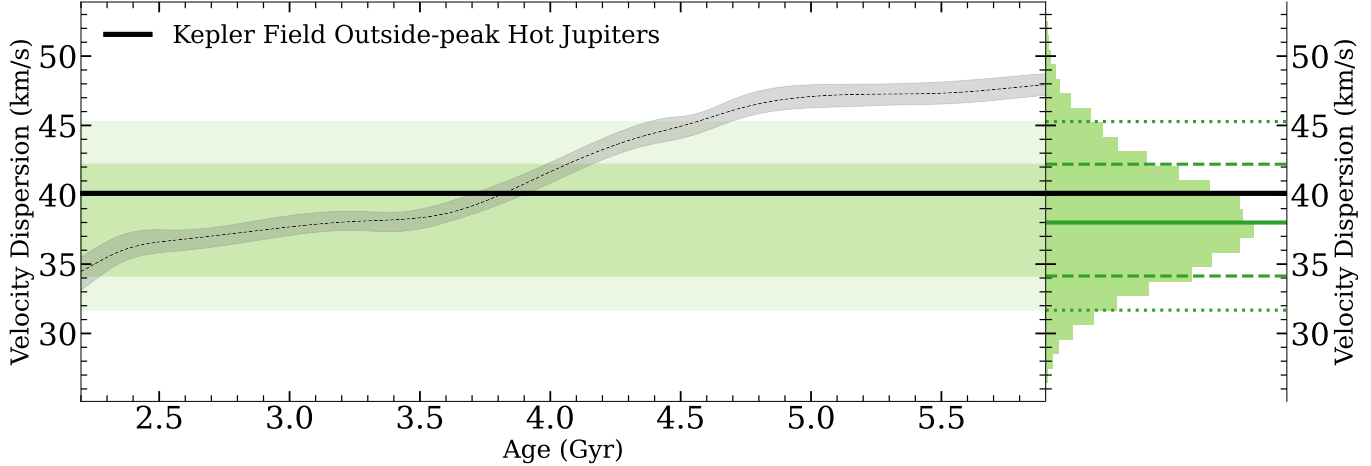


Figure 9. Velocity dispersions of Kepler-discovered outside-peak hot Jupiter host stars and matched control samples of Kepler field stars without transiting hot Jupiters. We follow the methodology presented in J. H. Hamer & K. C. Schlaufman (2019) and calculate velocity dispersions for both populations after constructing control samples of Kepler field stars matched in mass and metallicity to the host stars of Kepler-discovered outside-peak hot Jupiters using the T. A. Berger et al. (2020) catalog of stellar parameters. We plot as the black dashed line the S. P. Schmidt et al. (2024) Kepler field age–velocity dispersion and indicate its 16th/84th interquartile range in gray. We plot as the heavy black line at $\sigma \approx 40 \text{ km s}^{-1}$ the velocity dispersion of the sample of Kepler-discovered outside-peak hot Jupiter host stars. On the left, we plot the 16th/84th and 5th/95th interquartile ranges of the control sample velocity dispersion distribution as the green and light green rectangles. On the right, we plot a histogram of individual control sample velocity dispersions and indicate its median with a solid green line and its 16th/84th and 5th/95th interquartile ranges with horizontal green dashed and dotted lines. We find that the velocity dispersion of the sample of host stars of Kepler-discovered outside-peak hot Jupiters is fully consistent with the velocity dispersion distribution expected from matched control samples of Kepler field stars without transiting hot Jupiters. This consistency validates our interpretation of the results presented in this article as evidence that hot Jupiters outside the debiased peak of the hot Jupiter orbital period distribution arrived early in the evolution of their planetary systems and are subsequently survive tidal interactions while their host stars are on the main sequence.

5. CONCLUSION

Several hot Jupiter formation scenarios have been suggested to explain the existence of the observed peak in the hot Jupiter orbital period distribution. We propose that the relative ages of hot Jupiters inside, near, and outside the peak in the orbital period distribution can be used to distinguish between these suggested possibilities. We therefore split the population of transiting solar neighborhood hot Jupiter systems into three subpopulations inside, near, and outside the debiased orbital period peak and then use their Galactic velocity dispersions to infer their characteristic mean ages. We find that the outside-peak subpopulation ($4.545 \text{ d} < P_{\text{orb}} < 10 \text{ d}$) has a characteristic mean age in the range $2.20 \text{ Gyr} \lesssim \tau \lesssim 2.36 \text{ Gyr}$. On the other hand, we find that the near-peak subpopulation ($3.259 \text{ d} < P_{\text{orb}} < 4.545 \text{ d}$) and inside-peak subpopulation ($P_{\text{orb}} < 3.259 \text{ d}$) have characteristic mean ages in the ranges $3.11 \text{ Gyr} \lesssim \tau \lesssim 3.27 \text{ Gyr}$ and $3.16 \text{ Gyr} \lesssim \tau \lesssim 3.30 \text{ Gyr}$. These age offsets cannot be explained by differences in differing stellar mass distributions in each subpopulation. The older ages of the near- and inside-peak subpopulations suggest that

many of these systems are formed by a late-time, peak-populating formation mechanism like high-eccentricity migration. They are then sculpted by tidal inspiral over billions of years.

We create a parametric forward model of the evolution of the hot Jupiter population and find that Q'_* values in the range $10^{6.5} \lesssim Q'_* \lesssim 10^7$ quantitatively reproduce our observations. We further find that between 40% and 70% of the hot Jupiter population must have formed via a late-time, peak-populating mechanism with a characteristic post-formation timescale that exceeds 1.5 Gyr. When we consider more or less dissipative host stars for our model, while we find that Q'_* values in the range $10^6 \lesssim Q'_* \lesssim 10^{7.5}$ can qualitatively reproduce our observations, they cannot do so quantitatively. Our observations imply that most of the hot Jupiters near the debiased peak in the orbital period distribution are late arrivals that took more than 1.5 Gyr to become hot Jupiters. Hot Jupiters inside the debiased orbital period peak formed in a similar manner but have experienced more dynamically important tidal inspiral. In contrast, most hot Jupiters outside the debiased orbital peak formed via disk migration or in situ formation in a similar fashion to longer-period giant planets. Those

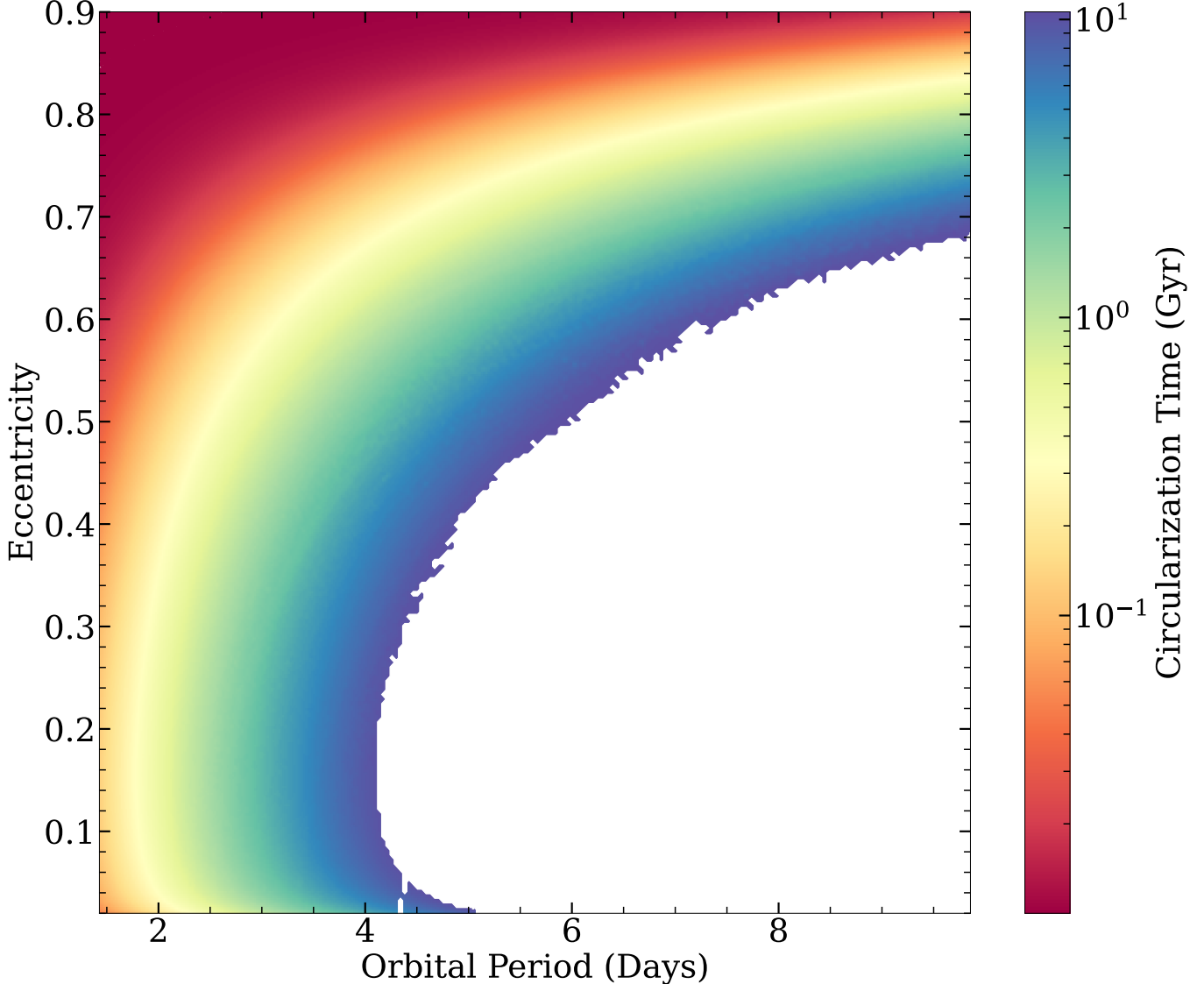


Figure 10. Circularization time as a function of initial orbital period and eccentricity for a $1 M_{\text{Jup}}$ planet orbiting a $1 M_{\odot}$ star using the J. Leconte et al. (2010) model assuming the rotational stellar evolution models presented in L. Amard et al. (2019) and a stellar obliquity of zero. We assume a planet tidal quality factor $Q'_p = 3.56 \times 10^5$ (V. Lainey et al. 2009) and a stellar tidal quality factor $Q'_* = 10^7$. The color bar indicates the time for a system's eccentricity to be tidally damped to $e < 0.01$ at which point it is observationally indistinguishable from $e = 0$. We indicate in white regions in which $e \geq 0.01$ for more than 10 Gyr. Since the peak of the debiased hot Jupiter orbital period distribution is near $P = 4$ d, we expect that many systems in our outside-peak subpopulation will not have fully circularized by the time their host stars leave the main sequence.

wide-separation systems survive tidal evolution for the duration of their host stars' main sequence lifetimes and can be observed transiting evolved post-main sequence stars.

ACKNOWLEDGMENTS

We thank the anonymous referee for their helpful comments. We thank Daniel Thorngren for a helpful comment about ODE integration for edge cases and Nicole Crumpler for a helpful comment about parallelization.

Stephen P. Schmidt is supported by the National Science Foundation Graduate Research Fellowship Program under Grant No. DGE2139757. This work has made use of data from the European Space Agency (ESA) mission *Gaia* (<https://www.cosmos.esa.int/gaia>), processed by the *Gaia* Data Processing and Analysis Consortium (DPAC, <https://www.cosmos.esa.int/web/gaia/dpac/consortium>). Funding for the DPAC has been provided by national institutions, in particular the institutions participating in the *Gaia* Multilateral Agreement. This research has made use of the SIM-

BAD database, operated at CDS, Strasbourg, France (M. Wenger et al. 2000). This research has made use of the VizieR catalog access tool, CDS, Strasbourg, France. The original description of the VizieR service was published in F. Ochsenbein et al. (2000). This research has made use of the NASA Exoplanet Archive (R. L. Akeson et al. 2013; J. L. Christiansen et al. 2025), which is operated by the California Institute of Technology, under contract with the National Aeronautics and Space Administration under the Exoplanet Exploration Program. Funding for SDSS-III has been provided by the Alfred P. Sloan Foundation, the Participating Institutions, the National Science Foundation, and the U.S. Department of Energy Office of Science. The SDSS-III web site is <http://www.sdss3.org/>. SDSS-III is managed by the Astrophysical Research Consortium for the Participating Institutions of the SDSS-III Collaboration including the University of Arizona, the Brazilian Participation Group, Brookhaven National Laboratory, Carnegie Mellon University, University of Florida, the French Participation Group, the German Participation Group, Harvard University, the Instituto de Astrofísica de Canarias, the Michigan State/Notre Dame/JINA Participation Group, Johns Hopkins University, Lawrence Berkeley National Laboratory, Max Planck Institute for Astrophysics, Max Planck Institute for Extraterrestrial Physics, New Mexico State University, New York University, Ohio State University, Pennsylvania State University, University of Portsmouth, Princeton University, the Spanish Participation Group, University of Tokyo, University of Utah, Vanderbilt University, University of Virginia, University of Washington, and Yale University. Funding for the Sloan Digital Sky Survey IV has been provided by the Alfred P. Sloan Foundation, the U.S. Department of Energy Office of Science, and the Participating Institutions. SDSS-IV acknowledges support and resources from the Center for High Performance Computing at the University of Utah. The SDSS website is www.sdss4.org. SDSS-IV is managed by the Astrophysical Research Consortium for the Participat-

ing Institutions of the SDSS Collaboration including the Brazilian Participation Group, the Carnegie Institution for Science, Carnegie Mellon University, Center for Astrophysics — Harvard & Smithsonian, the Chilean Participation Group, the French Participation Group, Instituto de Astrofísica de Canarias, The Johns Hopkins University, Kavli Institute for the Physics and Mathematics of the Universe (IPMU) / University of Tokyo, the Korean Participation Group, Lawrence Berkeley National Laboratory, Leibniz Institut für Astrophysik Potsdam (AIP), Max-Planck-Institut für Astronomie (MPIA Heidelberg), Max-Planck-Institut für Astrophysik (MPA Garching), Max-Planck-Institut für Extraterrestrische Physik (MPE), National Astronomical Observatories of China, New Mexico State University, New York University, University of Notre Dame, Observatório Nacional / MCTI, The Ohio State University, Pennsylvania State University, Shanghai Astronomical Observatory, United Kingdom Participation Group, Universidad Nacional Autónoma de México, University of Arizona, University of Colorado Boulder, University of Oxford, University of Portsmouth, University of Utah, University of Virginia, University of Washington, University of Wisconsin, Vanderbilt University, and Yale University. This research has made use of NASA’s Astrophysics Data System.

Facilities: ADS, CDS, Du Pont (APOGEE), Exoplanet Archive, Gaia, Sloan (APOGEE)

Software: `astropy` (Astropy Collaboration et al. 2013, 2018, 2022), `astroquery` (A. Ginsburg et al. 2019), `gaiadr3_zeropoint` (L. Lindegren et al. 2021a), `gala` (A. M. Price-Whelan 2017; A. Price-Whelan et al. 2020), `matplotlib` (J. D. Hunter 2007), `numpy` (C. R. Harris et al. 2020), `pandas` (Wes McKinney 2010; T. pandas development team 2020), `pyia` (A. Price-Whelan 2018), `scipy` (E. Jones et al. 2024; P. Virtanen et al. 2020), `TOPCAT` (M. B. Taylor 2005)

REFERENCES

Abdurro’uf, Accetta, K., Aerts, C., et al. 2022, ApJS, 259, 35, doi: [10.3847/1538-4365/ac4414](https://doi.org/10.3847/1538-4365/ac4414)

Akeson, R. L., Chen, X., Ciardi, D., et al. 2013, PASP, 125, 989, doi: [10.1086/672273](https://doi.org/10.1086/672273)

Allende Prieto, C., Beers, T. C., Wilhelm, R., et al. 2006, ApJ, 636, 804, doi: [10.1086/498131](https://doi.org/10.1086/498131)

Alvarez, R., & Plez, B. 1998, A&A, 330, 1109, doi: [10.48550/arXiv.astro-ph/9710157](https://arxiv.org/abs/astro-ph/9710157)

Amard, L., Palacios, A., Charbonnel, C., et al. 2019, A&A, 631, A77, doi: [10.1051/0004-6361/201935160](https://doi.org/10.1051/0004-6361/201935160)

Astropy Collaboration, Robitaille, T. P., Tollerud, E. J., et al. 2013, A&A, 558, A33, doi: [10.1051/0004-6361/201322068](https://doi.org/10.1051/0004-6361/201322068)

Astropy Collaboration, Price-Whelan, A. M., Sipőcz, B. M., et al. 2018, AJ, 156, 123, doi: [10.3847/1538-3881/aabc4f](https://doi.org/10.3847/1538-3881/aabc4f)

Astropy Collaboration, Price-Whelan, A. M., Lim, P. L., et al. 2022, ApJ, 935, 167, doi: [10.3847/1538-4357/ac7c74](https://doi.org/10.3847/1538-4357/ac7c74)

Aumer, M., & Binney, J. J. 2009, MNRAS, 397, 1286, doi: [10.1111/j.1365-2966.2009.15053.x](https://doi.org/10.1111/j.1365-2966.2009.15053.x)

Babusiaux, C., Fabricius, C., Khanna, S., et al. 2023, A&A, 674, A32, doi: [10.1051/0004-6361/202243790](https://doi.org/10.1051/0004-6361/202243790)

Batygin, K., Bodenheimer, P. H., & Laughlin, G. P. 2016, ApJ, 829, 114, doi: [10.3847/0004-637X/829/2/114](https://doi.org/10.3847/0004-637X/829/2/114)

Beaton, R. L., Oelkers, R. J., Hayes, C. R., et al. 2021, AJ, 162, 302, doi: [10.3847/1538-3881/ac260c](https://doi.org/10.3847/1538-3881/ac260c)

Beaugé, C., & Nesvorný, D. 2012, ApJ, 751, 119, doi: [10.1088/0004-637X/751/2/119](https://doi.org/10.1088/0004-637X/751/2/119)

Becker, J. C., Vanderburg, A., Adams, F. C., Rappaport, S. A., & Schwengeler, H. M. 2015, ApJL, 812, L18, doi: [10.1088/2041-8205/812/2/L18](https://doi.org/10.1088/2041-8205/812/2/L18)

Berger, T. A., Huber, D., van Saders, J. L., et al. 2020, AJ, 159, 280, doi: [10.3847/1538-3881/159/6/280](https://doi.org/10.3847/1538-3881/159/6/280)

Bieryla, A., Dong, J., Zhou, G., et al. 2025, AJ, 169, 273, doi: [10.3847/1538-3881/adc441](https://doi.org/10.3847/1538-3881/adc441)

Blanton, M. R., Bershady, M. A., Abolfathi, B., et al. 2017, AJ, 154, 28, doi: [10.3847/1538-3881/aa7567](https://doi.org/10.3847/1538-3881/aa7567)

Bodenheimer, P., Hubickyj, O., & Lissauer, J. J. 2000, Icarus, 143, 2, doi: [10.1006/icar.1999.6246](https://doi.org/10.1006/icar.1999.6246)

Bonomo, A. S., Desidera, S., Benatti, S., et al. 2017, A&A, 602, A107, doi: [10.1051/0004-6361/201629882](https://doi.org/10.1051/0004-6361/201629882)

Bovy, J. 2015, ApJS, 216, 29, doi: [10.1088/0067-0049/216/2/29](https://doi.org/10.1088/0067-0049/216/2/29)

Bryan, M. L., Knutson, H. A., Howard, A. W., et al. 2016, ApJ, 821, 89, doi: [10.3847/0004-637X/821/2/89](https://doi.org/10.3847/0004-637X/821/2/89)

Buhler, P. B., Knutson, H. A., Batygin, K., et al. 2016, ApJ, 821, 26, doi: [10.3847/0004-637X/821/1/26](https://doi.org/10.3847/0004-637X/821/1/26)

Chatterjee, S., Ford, E. B., Matsumura, S., & Rasio, F. A. 2008, ApJ, 686, 580, doi: [10.1086/590227](https://doi.org/10.1086/590227)

Chen, D.-C., Xie, J.-W., Zhou, J.-L., et al. 2021, ApJ, 909, 115, doi: [10.3847/1538-4357/abd5be](https://doi.org/10.3847/1538-4357/abd5be)

Chen, D.-C., Xie, J.-W., Zhou, J.-L., et al. 2023, Proceedings of the National Academy of Science, 120, e2304179120, doi: [10.1073/pnas.2304179120](https://doi.org/10.1073/pnas.2304179120)

Choi, J., Dotter, A., Conroy, C., et al. 2016, ApJ, 823, 102, doi: [10.3847/0004-637X/823/2/102](https://doi.org/10.3847/0004-637X/823/2/102)

Christiansen, J. L., McElroy, D. L., Harbut, M., et al. 2025, PSJ, 6, 186, doi: [10.3847/PSJ/ade3c2](https://doi.org/10.3847/PSJ/ade3c2)

Cunha, K., Smith, V. V., Johnson, J. A., et al. 2015, ApJL, 798, L41, doi: [10.1088/2041-8205/798/2/L41](https://doi.org/10.1088/2041-8205/798/2/L41)

Dotter, A. 2016, ApJS, 222, 8, doi: [10.3847/0067-0049/222/1/8](https://doi.org/10.3847/0067-0049/222/1/8)

Eisenstein, D. J., Weinberg, D. H., Agol, E., et al. 2011, AJ, 142, 72, doi: [10.1088/0004-6256/142/3/72](https://doi.org/10.1088/0004-6256/142/3/72)

Espinoza-Retamal, J. I., Brahm, R., Petrovich, C., et al. 2023, ApJL, 958, L20, doi: [10.3847/2041-8213/ad096d](https://doi.org/10.3847/2041-8213/ad096d)

Espinoza-Retamal, J. I., Jordán, A., Brahm, R., et al. 2025, AJ, 170, 70, doi: [10.3847/1538-3881/ade22e](https://doi.org/10.3847/1538-3881/ade22e)

Fabricius, C., Luri, X., Arenou, F., et al. 2021, A&A, 649, A5, doi: [10.1051/0004-6361/202039834](https://doi.org/10.1051/0004-6361/202039834)

Fabrycky, D. C., & Winn, J. N. 2009, ApJ, 696, 1230, doi: [10.1088/0004-637X/696/2/1230](https://doi.org/10.1088/0004-637X/696/2/1230)

Fischer, D. A., & Valenti, J. 2005, ApJ, 622, 1102, doi: [10.1086/428383](https://doi.org/10.1086/428383)

Fressin, F., Torres, G., Charbonneau, D., et al. 2013, ApJ, 766, 81, doi: [10.1088/0004-637X/766/2/81](https://doi.org/10.1088/0004-637X/766/2/81)

Gaia Collaboration, Prusti, T., de Bruijne, J. H. J., et al. 2016, A&A, 595, A1, doi: [10.1051/0004-6361/201629272](https://doi.org/10.1051/0004-6361/201629272)

Gaia Collaboration, Brown, A. G. A., Vallenari, A., et al. 2021, A&A, 649, A1, doi: [10.1051/0004-6361/202039657](https://doi.org/10.1051/0004-6361/202039657)

Gaia Collaboration, Klioner, S. A., Lindegren, L., et al. 2022, A&A, 667, A148, doi: [10.1051/0004-6361/202243483](https://doi.org/10.1051/0004-6361/202243483)

Gaia Collaboration, Vallenari, A., Brown, A. G. A., et al. 2023, A&A, 674, A1, doi: [10.1051/0004-6361/202243940](https://doi.org/10.1051/0004-6361/202243940)

García Pérez, A. E., Allende Prieto, C., Holtzman, J. A., et al. 2016, AJ, 151, 144, doi: [10.3847/0004-6256/151/6/144](https://doi.org/10.3847/0004-6256/151/6/144)

Gilliland, R. L., Brown, T. M., Guhathakurta, P., et al. 2000, ApJL, 545, L47, doi: [10.1086/317334](https://doi.org/10.1086/317334)

Ginsburg, A., Sipőcz, B. M., Brasseur, C. E., et al. 2019, AJ, 157, 98, doi: [10.3847/1538-3881/aafc33](https://doi.org/10.3847/1538-3881/aafc33)

Grumblatt, S. K., Saunders, N., Sun, M., et al. 2022, AJ, 163, 120, doi: [10.3847/1538-3881/ac4972](https://doi.org/10.3847/1538-3881/ac4972)

Grunblatt, S. K., Saunders, N., Chontos, A., et al. 2023, AJ, 165, 44, doi: [10.3847/1538-3881/aca670](https://doi.org/10.3847/1538-3881/aca670)

Gunn, J. E., Siegmund, W. A., Mannery, E. J., et al. 2006, AJ, 131, 2332, doi: [10.1086/500975](https://doi.org/10.1086/500975)

Gupta, A. F., Millholland, S. C., Im, H., et al. 2024, Nature, 632, 50, doi: [10.1038/s41586-024-07688-3](https://doi.org/10.1038/s41586-024-07688-3)

Gustafsson, B., Edvardsson, B., Eriksson, K., et al. 2008, A&A, 486, 951, doi: [10.1051/0004-6361:200809724](https://doi.org/10.1051/0004-6361:200809724)

Hamer, J. H., & Schlaufman, K. C. 2019, AJ, 158, 190, doi: [10.3847/1538-3881/ab3c56](https://doi.org/10.3847/1538-3881/ab3c56)

Hamer, J. H., & Schlaufman, K. C. 2020, AJ, 160, 138, doi: [10.3847/1538-3881/aba74f](https://doi.org/10.3847/1538-3881/aba74f)

Hamer, J. H., & Schlaufman, K. C. 2022, AJ, 164, 26, doi: [10.3847/1538-3881/ac69ef](https://doi.org/10.3847/1538-3881/ac69ef)

Hamer, J. H., & Schlaufman, K. C. 2024, AJ, 167, 55, doi: [10.3847/1538-3881/ad110e](https://doi.org/10.3847/1538-3881/ad110e)

Harris, C. R., Millman, K. J., van der Walt, S. J., et al. 2020, Nature, 585, 357, doi: [10.1038/s41586-020-2649-2](https://doi.org/10.1038/s41586-020-2649-2)

Holman, M., Touma, J., & Tremaine, S. 1997, Nature, 386, 254, doi: [10.1038/386254a0](https://doi.org/10.1038/386254a0)

Holtzman, J. A., Harrison, T. E., & Coughlin, J. L. 2010, Advances in Astronomy, 2010, 193086, doi: [10.1155/2010/193086](https://doi.org/10.1155/2010/193086)

Holtzman, J. A., Shetrone, M., Johnson, J. A., et al. 2015, AJ, 150, 148, doi: [10.1088/0004-6256/150/5/148](https://doi.org/10.1088/0004-6256/150/5/148)

Hord, B. J., Colón, K. D., Berger, T. A., et al. 2022, AJ, 164, 13, doi: [10.3847/1538-3881/ac6f57](https://doi.org/10.3847/1538-3881/ac6f57)

Hu, Q., Rice, M., Wang, X.-Y., et al. 2024, AJ, 167, 175, doi: [10.3847/1538-3881/ad2855](https://doi.org/10.3847/1538-3881/ad2855)

Hubeny, I., & Lanz, T. 2011,, Astrophysics Source Code Library, record ascl:1109.022

Hubickyj, O., Bodenheimer, P., & Lissauer, J. J. 2005, Icarus, 179, 415, doi: [10.1016/j.icarus.2005.06.021](https://doi.org/10.1016/j.icarus.2005.06.021)

Hunter, J. D. 2007, Computing in science & engineering, 9, 90

Jackson, B., Greenberg, R., & Barnes, R. 2008, ApJ, 678, 1396, doi: [10.1086/529187](https://doi.org/10.1086/529187)

Jackson, J. M., Dawson, R. I., Quarles, B., & Dong, J. 2023, AJ, 165, 82, doi: [10.3847/1538-3881/acac86](https://doi.org/10.3847/1538-3881/acac86)

Jermyn, A. S., Bauer, E. B., Schwab, J., et al. 2023, ApJS, 265, 15, doi: [10.3847/1538-4365/aca8d](https://doi.org/10.3847/1538-4365/aca8d)

Jones, E., Oliphant, T., Peterson, P., et al. 2024, <http://www.scipy.org/>

Jönsson, H., Holtzman, J. A., Allende Prieto, C., et al. 2020, AJ, 160, 120, doi: [10.3847/1538-3881/aba592](https://doi.org/10.3847/1538-3881/aba592)

Katz, D., Sartoretti, P., Guerrier, A., et al. 2023, A&A, 674, A5, doi: [10.1051/0004-6361/202244220](https://doi.org/10.1051/0004-6361/202244220)

Kipping, D. M. 2013, MNRAS, 434, L51, doi: [10.1093/mnrasl/slt075](https://doi.org/10.1093/mnrasl/slt075)

Kiseleva, L. G., Eggleton, P. P., & Mikkola, S. 1998, MNRAS, 300, 292, doi: [10.1046/j.1365-8711.1998.01903.x](https://doi.org/10.1046/j.1365-8711.1998.01903.x)

Knudstrup, E., & Albrecht, S. H. 2022, A&A, 660, A99, doi: [10.1051/0004-6361/202142726](https://doi.org/10.1051/0004-6361/202142726)

Knutson, H. A., Fulton, B. J., Montet, B. T., et al. 2014, ApJ, 785, 126, doi: [10.1088/0004-637X/785/2/126](https://doi.org/10.1088/0004-637X/785/2/126)

Lainey, V., Arlot, J.-E., Karatekin, Ö., & van Hoolst, T. 2009, Nature, 459, 957, doi: [10.1038/nature08108](https://doi.org/10.1038/nature08108)

Leconte, J., Chabrier, G., Baraffe, I., & Levrard, B. 2010, A&A, 516, A64, doi: [10.1051/0004-6361/201014337](https://doi.org/10.1051/0004-6361/201014337)

Lin, D. N. C., Bodenheimer, P., & Richardson, D. C. 1996, Nature, 380, 606, doi: [10.1038/380606a0](https://doi.org/10.1038/380606a0)

Lindegren, L., Bastian, U., Biermann, M., et al. 2021a, A&A, 649, A4, doi: [10.1051/0004-6361/202039653](https://doi.org/10.1051/0004-6361/202039653)

Lindegren, L., Klioner, S. A., Hernández, J., et al. 2021b, A&A, 649, A2, doi: [10.1051/0004-6361/202039709](https://doi.org/10.1051/0004-6361/202039709)

Lubin, J., Wang, X.-Y., Rice, M., et al. 2023, ApJL, 959, L5, doi: [10.3847/2041-8213/ad0fea](https://doi.org/10.3847/2041-8213/ad0fea)

Majewski, S. R., Schiavon, R. P., Frinchaboy, P. M., et al. 2017, AJ, 154, 94, doi: [10.3847/1538-3881/aa784d](https://doi.org/10.3847/1538-3881/aa784d)

Marcy, G. W., Butler, R. P., Vogt, S. S., et al. 2005, ApJ, 619, 570, doi: [10.1086/426384](https://doi.org/10.1086/426384)

Marrese, P. M., Marinoni, S., Fabrizio, M., & Altavilla, G. 2021,, Gaia EDR3 documentation, European Space Agency; Gaia Data Processing and Analysis Consortium. Online at [jA href="https://gea.esac.esa.int/archive/documentation/GEDR3/index.html">id. 9](https://gea.esac.esa.int/archive/documentation/GEDR3/index.html)

Marrese, P. M., Marinoni, S., Fabrizio, M., & Altavilla, G. 2022,, Gaia DR3 documentation, European Space Agency; Gaia Data Processing and Analysis Consortium. Online at [jA href="https://gea.esac.esa.int/archive/documentation/GDR3/index.html">id. 15](https://gea.esac.esa.int/archive/documentation/GDR3/index.html)

Mayor, M., Marmier, M., Lovis, C., et al. 2011, arXiv e-prints, arXiv:1109.2497, doi: [10.48550/arXiv.1109.2497](https://doi.org/10.48550/arXiv.1109.2497)

Mazeh, T., Krymolowski, Y., & Rosenfeld, G. 1997, ApJL, 477, L103, doi: [10.1086/310536](https://doi.org/10.1086/310536)

Miyazaki, S., & Masuda, K. 2023, AJ, 166, 209, doi: [10.3847/1538-3881/acff71](https://doi.org/10.3847/1538-3881/acff71)

Moe, M., & Kratter, K. M. 2021, MNRAS, 507, 3593, doi: [10.1093/mnras/stab2328](https://doi.org/10.1093/mnras/stab2328)

Morton, T. D., & Johnson, J. A. 2011, ApJ, 729, 138, doi: [10.1088/0004-637X/729/2/138](https://doi.org/10.1088/0004-637X/729/2/138)

Muñoz, D. J., Lai, D., & Liu, B. 2016, MNRAS, 460, 1086, doi: [10.1093/mnras/stw983](https://doi.org/10.1093/mnras/stw983)

Naef, D., Latham, D. W., Mayor, M., et al. 2001, A&A, 375, L27, doi: [10.1051/0004-6361:20010853](https://doi.org/10.1051/0004-6361:20010853)

Nagasawa, M., Ida, S., & Bessho, T. 2008, ApJ, 678, 498, doi: [10.1086/529369](https://doi.org/10.1086/529369)

Naoz, S., Farr, W. M., & Rasio, F. A. 2012, ApJL, 754, L36, doi: [10.1088/2041-8205/754/2/L36](https://doi.org/10.1088/2041-8205/754/2/L36)

NASA Exoplanet Archive. 2025,, Version: 2025-07-2 NExScI-Caltech/IPAC, doi: [10.26133/NEA13](https://doi.org/10.26133/NEA13)

Nataf, D. M., Schlaufman, K. C., Reggiani, H., & Hahn, I. 2024, ApJ, 976, 87, doi: [10.3847/1538-4357/ad7c4e](https://doi.org/10.3847/1538-4357/ad7c4e)

Nelson, B. E., Ford, E. B., & Rasio, F. A. 2017, AJ, 154, 106, doi: [10.3847/1538-3881/aa82b3](https://doi.org/10.3847/1538-3881/aa82b3)

Ngo, H., Knutson, H. A., Hinkley, S., et al. 2016, ApJ, 827, 8, doi: [10.3847/0004-637X/827/1/8](https://doi.org/10.3847/0004-637X/827/1/8)

Nidever, D. L., Holtzman, J. A., Allende Prieto, C., et al. 2015, AJ, 150, 173, doi: [10.1088/0004-6256/150/6/173](https://doi.org/10.1088/0004-6256/150/6/173)

Ochsenbein, F., Bauer, P., & Marcout, J. 2000, A&AS, 143, 23, doi: [10.1051/aas:2000169](https://doi.org/10.1051/aas:2000169)

pandas development team, T. 2020,, 1.5.0 Zenodo, doi: [10.5281/zenodo.3509134](https://doi.org/10.5281/zenodo.3509134)

Paxton, B., Bildsten, L., Dotter, A., et al. 2011, ApJS, 192, 3, doi: [10.1088/0067-0049/192/1/3](https://doi.org/10.1088/0067-0049/192/1/3)

Paxton, B., Cantiello, M., Arras, P., et al. 2013, ApJS, 208, 4, doi: [10.1088/0067-0049/208/1/4](https://doi.org/10.1088/0067-0049/208/1/4)

Paxton, B., Schwab, J., Bauer, E. B., et al. 2018, ApJS, 234, 34, doi: [10.3847/1538-4365/aaa5a8](https://doi.org/10.3847/1538-4365/aaa5a8)

Paxton, B., Smolec, R., Schwab, J., et al. 2019, *ApJS*, 243, 10, doi: [10.3847/1538-4365/ab2241](https://doi.org/10.3847/1538-4365/ab2241)

Pereira, F., Grunblatt, S. K., Psaridi, A., et al. 2024, *MNRAS*, 527, 6332, doi: [10.1093/mnras/stad3449](https://doi.org/10.1093/mnras/stad3449)

Petrovich, C. 2015, *ApJ*, 805, 75, doi: [10.1088/0004-637X/805/1/75](https://doi.org/10.1088/0004-637X/805/1/75)

Plavchan, P., & Bilinski, C. 2013, *ApJ*, 769, 86, doi: [10.1088/0004-637X/769/2/86](https://doi.org/10.1088/0004-637X/769/2/86)

Plez, B. 2012,, Astrophysics Source Code Library, record ascl:1205.004

Pollack, J. B., Hubickyj, O., Bodenheimer, P., et al. 1996, *Icarus*, 124, 62, doi: [10.1006/icar.1996.0190](https://doi.org/10.1006/icar.1996.0190)

Price-Whelan, A. 2018,, v0.2 Zenodo, doi: [10.5281/zenodo.1228136](https://doi.org/10.5281/zenodo.1228136)

Price-Whelan, A., Sipőcz, B., Lenz, D., et al. 2020,, v1.8.1 Zenodo, doi: [10.5281/zenodo.4159870](https://doi.org/10.5281/zenodo.4159870)

Price-Whelan, A. M. 2017, *The Journal of Open Source Software*, 2, doi: [10.21105/joss.00388](https://doi.org/10.21105/joss.00388)

Rasio, F. A., & Ford, E. B. 1996, *Science*, 274, 954, doi: [10.1126/science.274.5289.954](https://doi.org/10.1126/science.274.5289.954)

Rasio, F. A., Tout, C. A., Lubow, S. H., & Livio, M. 1996, *ApJ*, 470, 1187, doi: [10.1086/177941](https://doi.org/10.1086/177941)

Rice, M., Wang, S., & Laughlin, G. 2022a, *ApJL*, 926, L17, doi: [10.3847/2041-8213/ac502d](https://doi.org/10.3847/2041-8213/ac502d)

Rice, M., Wang, S., Wang, X.-Y., et al. 2022b, *AJ*, 164, 104, doi: [10.3847/1538-3881/ac8153](https://doi.org/10.3847/1538-3881/ac8153)

Ricker, G. R., Winn, J. N., Vanderspek, R., et al. 2014, in Society of Photo-Optical Instrumentation Engineers (SPIE) Conference Series, Vol. 9143, Space Telescopes and Instrumentation 2014: Optical, Infrared, and Millimeter Wave, ed. J. M. Oschmann, Jr., M. Clampin, G. G. Fazio, & H. A. MacEwen, 914320, doi: [10.1117/12.2063489](https://doi.org/10.1117/12.2063489)

Riello, M., De Angelis, F., Evans, D. W., et al. 2021, *A&A*, 649, A3, doi: [10.1051/0004-6361/202039587](https://doi.org/10.1051/0004-6361/202039587)

Rowell, N., Davidson, M., Lindegren, L., et al. 2021, *A&A*, 649, A11, doi: [10.1051/0004-6361/202039448](https://doi.org/10.1051/0004-6361/202039448)

Santana, F. A., Beaton, R. L., Covey, K. R., et al. 2021, *AJ*, 162, 303, doi: [10.3847/1538-3881/ac2cbc](https://doi.org/10.3847/1538-3881/ac2cbc)

Santerne, A., Díaz, R. F., Moutou, C., et al. 2012, *A&A*, 545, A76, doi: [10.1051/0004-6361/201219608](https://doi.org/10.1051/0004-6361/201219608)

Santerne, A., Moutou, C., Tsantaki, M., et al. 2016, *A&A*, 587, A64, doi: [10.1051/0004-6361/201527329](https://doi.org/10.1051/0004-6361/201527329)

Santos, N. C., Israelian, G., & Mayor, M. 2004, *A&A*, 415, 1153, doi: [10.1051/0004-6361:20034469](https://doi.org/10.1051/0004-6361:20034469)

Saunders, N., Grunblatt, S. K., Huber, D., et al. 2022, *AJ*, 163, 53, doi: [10.3847/1538-3881/ac38a1](https://doi.org/10.3847/1538-3881/ac38a1)

Saunders, N., Grunblatt, S. K., Huber, D., et al. 2025, *AJ*, 169, 75, doi: [10.3847/1538-3881/ad9a87](https://doi.org/10.3847/1538-3881/ad9a87)

Schlafman, K. C. 2010, *ApJ*, 719, 602, doi: [10.1088/0004-637X/719/1/602](https://doi.org/10.1088/0004-637X/719/1/602)

Schlafman, K. C. 2018, *ApJ*, 853, 37, doi: [10.3847/1538-4357/aa961c](https://doi.org/10.3847/1538-4357/aa961c)

Schlafman, K. C., & Winn, J. N. 2016, *ApJ*, 825, 62, doi: [10.3847/0004-637X/825/1/62](https://doi.org/10.3847/0004-637X/825/1/62)

Schmidt, S. P., Schlafman, K. C., & Hamer, J. H. 2024, *AJ*, 168, 109, doi: [10.3847/1538-3881/ad5d76](https://doi.org/10.3847/1538-3881/ad5d76)

Schulte, J., Rodriguez, J. E., Bieryla, A., et al. 2024, *AJ*, 168, 32, doi: [10.3847/1538-3881/ad4a57](https://doi.org/10.3847/1538-3881/ad4a57)

Sedaghati, E., Jordán, A., Brahm, R., et al. 2023, *AJ*, 166, 130, doi: [10.3847/1538-3881/ace84](https://doi.org/10.3847/1538-3881/ace84)

Shetrone, M., Bizyaev, D., Lawler, J. E., et al. 2015, *ApJS*, 221, 24, doi: [10.1088/0067-0049/221/2/24](https://doi.org/10.1088/0067-0049/221/2/24)

Sing, D. K., Rustamkulov, Z., Thorngren, D. P., et al. 2024, *Nature*, 630, 831, doi: [10.1038/s41586-024-07395-z](https://doi.org/10.1038/s41586-024-07395-z)

Smith, V. V., Cunha, K., Shetrone, M. D., et al. 2013, *ApJ*, 765, 16, doi: [10.1088/0004-637X/765/1/16](https://doi.org/10.1088/0004-637X/765/1/16)

Smith, V. V., Bizyaev, D., Cunha, K., et al. 2021, *AJ*, 161, 254, doi: [10.3847/1538-3881/abefdc](https://doi.org/10.3847/1538-3881/abefdc)

Stassun, K. G., Oelkers, R. J., Paegert, M., et al. 2019, *AJ*, 158, 138, doi: [10.3847/1538-3881/ab3467](https://doi.org/10.3847/1538-3881/ab3467)

Taylor, M. B. 2005, in *Astronomical Society of the Pacific Conference Series*, Vol. 347, *Astronomical Data Analysis Software and Systems XIV*, ed. P. Shopbell, M. Britton, & R. Ebert, 29

Torra, F., Castañeda, J., Fabricius, C., et al. 2021, *A&A*, 649, A10, doi: [10.1051/0004-6361/202039637](https://doi.org/10.1051/0004-6361/202039637)

Virtanen, P., Gommers, R., Oliphant, T. E., et al. 2020, *Nature Methods*, 17, 261, doi: [10.1038/s41592-019-0686-2](https://doi.org/10.1038/s41592-019-0686-2)

Wang, S., Winn, J. N., Addison, B. C., et al. 2021, *AJ*, 162, 50, doi: [10.3847/1538-3881/ac0626](https://doi.org/10.3847/1538-3881/ac0626)

Wang, X.-Y., Rice, M., Wang, S., et al. 2024, *ApJL*, 973, L21, doi: [10.3847/2041-8213/ad7469](https://doi.org/10.3847/2041-8213/ad7469)

Ward, W. R. 1997, *Icarus*, 126, 261, doi: [10.1006/icar.1996.5647](https://doi.org/10.1006/icar.1996.5647)

Weidenschilling, S. J., & Marzari, F. 1996, *Nature*, 384, 619, doi: [10.1038/384619a0](https://doi.org/10.1038/384619a0)

Welbanks, L., Bell, T. J., Beatty, T. G., et al. 2024, *Nature*, 630, 836, doi: [10.1038/s41586-024-07514-w](https://doi.org/10.1038/s41586-024-07514-w)

Wenger, M., Ochsenbein, F., Egret, D., et al. 2000, *A&AS*, 143, 9, doi: [10.1051/aas:2000332](https://doi.org/10.1051/aas:2000332)

Wes McKinney. 2010, in *Proceedings of the 9th Python in Science Conference*, ed. Stéfan van der Walt & Jarrod Millman, 56 – 61, doi: [10.25080/Majora-92bf1922-00a](https://doi.org/10.25080/Majora-92bf1922-00a)

Wilson, J. C., Hearty, F. R., Skrutskie, M. F., et al. 2019, *PASP*, 131, 055001, doi: [10.1088/1538-3873/ab0075](https://doi.org/10.1088/1538-3873/ab0075)

Winn, J. N., Fabrycky, D., Albrecht, S., & Johnson, J. A. 2010, *ApJL*, 718, L145, doi: [10.1088/2041-8205/718/2/L145](https://doi.org/10.1088/2041-8205/718/2/L145)

Wright, J., Rice, M., Wang, X.-Y., Hixenbaugh, K., & Wang, S. 2023, AJ, 166, 217, doi: [10.3847/1538-3881/ad0131](https://doi.org/10.3847/1538-3881/ad0131)

Wright, J. T., Marcy, G. W., Howard, A. W., et al. 2012, ApJ, 753, 160, doi: [10.1088/0004-637X/753/2/160](https://doi.org/10.1088/0004-637X/753/2/160)

Wu, Y., & Lithwick, Y. 2011, ApJ, 735, 109, doi: [10.1088/0004-637X/735/2/109](https://doi.org/10.1088/0004-637X/735/2/109)

Wu, Y., & Murray, N. 2003, ApJ, 589, 605, doi: [10.1086/374598](https://doi.org/10.1086/374598)

Xiang, M., & Rix, H.-W. 2022, Nature, 603, 599, doi: [10.1038/s41586-022-04496-5](https://doi.org/10.1038/s41586-022-04496-5)

Yee, S. W., Winn, J. N., & Hartman, J. D. 2021, AJ, 162, 240, doi: [10.3847/1538-3881/ac2958](https://doi.org/10.3847/1538-3881/ac2958)

Yee, S. W., Winn, J. N., Hartman, J. D., et al. 2022, AJ, 164, 70, doi: [10.3847/1538-3881/ac73ff](https://doi.org/10.3847/1538-3881/ac73ff)

Yee, S. W., Winn, J. N., Hartman, J. D., et al. 2023, ApJS, 265, 1, doi: [10.3847/1538-4365/aca286](https://doi.org/10.3847/1538-4365/aca286)

Yee, S. W., Winn, J. N., Hartman, J. D., et al. 2025, ApJS, 280, 30, doi: [10.3847/1538-4365/aded0d](https://doi.org/10.3847/1538-4365/aded0d)

Zasowski, G., Johnson, J. A., Frinchaboy, P. M., et al. 2013, AJ, 146, 81, doi: [10.1088/0004-6256/146/4/81](https://doi.org/10.1088/0004-6256/146/4/81)

Zasowski, G., Cohen, R. E., Chojnowski, S. D., et al. 2017, AJ, 154, 198, doi: [10.3847/1538-3881/aa8df9](https://doi.org/10.3847/1538-3881/aa8df9)

Ziegler, C., Tokovinin, A., Briceño, C., et al. 2020, AJ, 159, 19, doi: [10.3847/1538-3881/ab55e9](https://doi.org/10.3847/1538-3881/ab55e9)